

VORTEX GENERATOR DESIGN FOR HIGH SUBSONIC INLETS

A THESIS SUBMITTED TO
THE GRADUATE SCHOOL OF NATURAL AND APPLIED SCIENCES
OF
MIDDLE EAST TECHNICAL UNIVERSITY

BY

BATUHAN NASUHBEOĞLU

IN PARTIAL FULFILLMENT OF THE REQUIREMENTS
FOR
THE DEGREE OF MASTER OF SCIENCE
IN
MECHANICAL ENGINEERING

SEPTEMBER 2014

Approval of the thesis

VORTEX GENERATOR DESIGN FOR HIGH SUBSONIC INLETS

submitted by **BATUHAN NASUHBEOĞLU** in partial fulfillment of the requirements for the degree of **Master of Science in Mechanical Engineering Department, Middle East Technical University** by,

Prof. Dr. Canan Özgen
Dean, Graduate School of **Natural and Applied Sciences**

Prof. Dr. Suha Oral
Head of Department, **Mechanical Engineering**

Prof. Dr. Kahraman Albayrak
Supervisor, **Mechanical Engineering Dept., METU**

Examining Committee Members:

Assoc. Prof. Cemil Yamalı
Mechanical Engineering Dept., METU

Prof. Dr. Kahraman Albayrak
Mechanical Engineering Dept., METU

Assoc. Prof. Dr. Metin Yavuz
Mechanical Engineering Dept., METU

Asst. Prof. Dr. Cüneyt Sert
Mechanical Engineering Dept., METU

Dr. Kemal Atılğan Toker
Chief Engineer, ROKETSAN

Date: 04/09/2014

I hereby declare that all the information in this document has been obtained and presented in accordance with academic rules and ethical conduct. I also declare that, as required by these rules and conduct, I have fully cited and referenced all material and results that are not original to this work.

Name, Last name : Batuhan NASUHBEOĞLU

Signature :

ABSTRACT

VORTEX GENERATOR DESIGN FOR SUBSONIC INLETS

Nasuhbeyođlu, Batuhan
M.S., Department of Mechanical Engineering
Supervisor: Prof. Dr. Kahraman Albayrak

September 2014, 69 Pages

In this thesis, numerical investigation of the benefits of vortex generators control on the performance of S-shaped inlets has been performed. This study is divided into two main parts. In the first part, a diffusive S-shaped inlet is examined and the numerical analyses results are compared with the experimental results. Three-dimensional Navier-Stokes equations are solved and three different turbulence models which are Realizable k- ϵ , Standard k- ω , and Spalart-Allmaras methods are used. Distortion coefficient and pressure recovery results at aerodynamic interface plane (AIP) are compared with experimental results and both of them are in good agreement. In the second part, a parametric design study for vortex generators are carried out in order to investigate possible effects of vortex generators on performance of the inlet, and results of the analyses are compared with the inlet without vortex generators. Inlet performance parameters which evaluate vortex generator efficiency are pressure recovery, distortion coefficient and mass flow rate at AIP. Several parameters such as device size, quantity and location are analyzed and an optimal configuration is chosen. Improvement on flow is observed for most of the configurations. For these configurations, value of pressure recovery is insignificantly reduced. On the other hand, there is a huge amount of improvement on distortion coefficient value. The aim of this study is to obtain a uniform flow as

much as possible at engine interface plane with no or negligible amount of mass flow rate loss. More uniform flow is obtained by reducing the value of distortion coefficient and the amount of pressure recovery loss due to vortex generators is also acceptable in terms of mass flow rate loss.

Keywords: Computational Fluid Dynamics, Vortex Generators, Distortion Coefficient, Pressure Recovery, S-Shaped Inlet, FLUENT

ÖZ

SES-ALTI HAVA ALIKLARINDA GİRDAP OLUŞTURMA AYGITI TASARIMI

Nasuhbeyođlu, Batuhan
Yüksek Lisans, Makina Mühendisliđi Bölümü
Tez Yöneticisi: Prof. Dr. Kahraman Albayrak

Eylül 2014, 69 Sayfa

Bu tezde, girdap oluřturma aygıtlarının S-řekilli hava alıklarının performansı üzerindeki sayısal etkileri incelenmiřtir. Bu çalıřma iki ana konuya ayrılmıřtır. Çalıřmanın ilk kısmında S-řekilli hava alıđı incelenmiř, analiz sonuçları deney verileriyle karřılařtırılmıřtır. Üç boyutlu Navier-Stokes denklemleri çözülmüř ve üç farklı türbülans modeli (Realizable $k-\epsilon$, Standard $k-\omega$, ve Spalart-Allmaras metodları) denenmiřtir. Analizlerde aerodinamik arayüzeyi üzerinde elde edilen bozulma katsayısı ve basınç korunumu deđerleri deney verileriyle karřılařtırılmıř, iki deđer için de birbiriyle örtüřen sonuçlar elde edilmiřtir. Tezin ikinci kısmında ise girdap oluřturma aygıtlarının hava alıđı performansı üzerindeki muhtemel etkilerini anlamak için girdap oluřturma aygıtları için parametrik tasarım çalıřması yapılmıř, analiz sonuçları ile üzerinde girdap oluřturma aygıtı bulunmayan hava alıđı analiz sonuçları karřılařtırılmıřtır. Aerodinamik arayüzeyi üzerinde hesaplanan basınç korunumu, bozuntu katsayısı ve kütle akıř oranı bařlıca performans parametreleridir. Aygıt boyutu, sayısı ve konumu gibi çeřitli parametreler analiz edilmiř, aralarında optimum performansı gösteren bir tasarım seçilmiřtir. Seçilen konfigürasyon için basınç korunumu ihmal edilebilir mertebelerde düřerken, bozuntu katsayısı deđerinde önemli bir iyileřtirme gözlemlenmiřtir. Bu tezin amacı motor arayüzünde minimum düzeyde kütle akıř oranı kaybıyla tekbiçimli akıř elde etmektir. Bozuntu

katsayısını dűşürerek daha tekbiçimli akış elde edilmiştir. Girdap oluřturma aygıtlarının sebep olduđu basınç korunumu katsayısındaki dűřüş ise kabul edilebilir mertebelerdedir.

Anahtar Kelimeler: Hesaplmalı Akışkanlar Dinamiđi, Girdap Oluřturma Aygıtları, Bozuntu Katsayısı, Basınç Korunumu, S-Şekilli Hava Alıđı, FLUENT

To My Family

ACKNOWLEDGEMENTS

I would like to express my appreciation and deepest gratitude to my supervisor Prof. Dr. Kahraman Albayrak for his guidance, advice, criticism and encouragements throughout the thesis.

I would also like to thank my manager Mr. Ali Akgül for his advices and criticism. I also want to thank my colleagues in Aerodynamics Department of ROKETSAN for all their help and support during the thesis.

I am very thankful to my parents Mrs. Nesrin Nasuhbeyođlu, Mr. Nasuh Mukbil Nasubeyođlu and my sister Mrs. Burcu Karaman for their help and motivation. Without them this work would not be completed.

I want to express my best wishes to Mr. Erhan Feyziođlu, Mr. Tolga Aydođdu, Mr. Abdullah Emre etiner and Mr. Engin ner for their friendship and support during this study.

TABLE OF CONTENTS

ABSTRACT	v
ÖZ	vii
ACKNOWLEDGEMENTS	x
TABLE OF CONTENTS	xi
LIST OF FIGURES	xiii
LIST OF TABLES	xvi
CHAPTERS	
1. INTRODUCTION	1
1.1 Flow Control	3
1.1.1 Closed Loop Flow Control	3
1.1.2 Open Loop Flow Control	3
1.2 Aim of the Thesis	5
1.3 Literature Survey	6
2. METHODOLOGY	13
2.1 Governing Equations	13
2.1.1 Fluid Modeling	13
2.2 Numerical Tool and Discretization	14
2.2.1 Grid Generation	15
2.2.2 Flow Solver	15
2.2.3 Discretization	16
2.2.4 Turbulence Modeling	17
2.3 Inlet Performance Parameters	23
2.3.1 Mass Flow Rate	23
2.3.2 Corrected Mass Flow Rate	24
2.3.3 Pressure Recovery	24
2.3.4 Distortion Coefficient	25
3. VALIDATION OF AERODYNAMIC MODEL	27
3.1 Inlet-A Test Case	27
3.2 Numerical Simulation	30
3.2.1 Solid Model	30
3.2.2 Mesh Independence Study	33

3.2.3	Turbulence Model Selection Study	35
3.2.4	Solution Domain Flow Visualization.....	37
4.	RESULTS.....	39
4.1	Solid Model and Mesh Generation	39
4.2	Solution.....	41
4.3	Results and Discussion	41
4.3.1	Vortex Generators	42
4.4	Post Process	59
5.	CONCLUSION AND FUTURE WORK.....	65
5.1	Conclusion.....	65
5.2	Future Work	66
	REFERENCES	67

LIST OF FIGURES

FIGURES

Figure 1-1 S-duct Inlet	1
Figure 1-2 Representation of Secondary Flow Forming.....	2
Figure 1-3 Vortex Generator Sample.....	4
Figure 1-4 Air Intake and Vortex Generator [5]	6
Figure 1-5 Co-rotating and Counter-Rotating Vortex Generators [9]	8
Figure 1-6 (a) Wheeler Vortex Generators, (b) Kuethe Vortex Generators [22].....	10
Figure 1-7 Fishtail Shaped Submerged Vortex Generator [2]	11
Figure 2-1 Overview of the Density-Based Solution Method	16
Figure 2-2 An Example of Control Volume Used for Discretization of a Scalar Transport Equation.....	17
Figure 2-3 Numerical Methods for Turbulence Modeling.....	18
Figure 2-4 The Near-Wall Region with Separated Layers.....	22
Figure 2-5 Near-Wall Region Models (a) Wall Function Approach, (b) Near-Wall Model Approach.....	22
Figure 2-6 AIP section	24
Figure 2-7 15° and 60° Pieces on AIP	25
Figure 2-7 Calculation of 60° Pieces on AIP.....	26
Figure 3-1 Geometry of Inlet-A [26]	28
Figure 3-2 Photograph of Inlet Model Mounted on Tunnel Sidewall. [8].....	28
Figure 3-3 Locations of Static Pressure Orifices on Inlet Walls [26]	29
Figure 3-4 Probes at AIP [26]	30
Figure 3-5 Solid Model of Inlet-A	30
Figure 3-6 Solution Domain.....	31
Figure 3-7 Corrected Mass Flow Rate Change for Different Mesh Qualities	32
Figure 3-8 Corrected Mass Flow Rate Change for Different Turbulence Models	33
Figure 3-9 Coarse, Medium and Fine Mesh.....	34
Figure 3-10 Pressure Recovery at AIP for Three Different Mesh Quality	35

Figure 3-11 Distortion Coefficient at AIP for Three Different Mesh Quality ($m_{corrected}=0.46$ kg/s).....	35
Figure 3-12 Pressure Recovery at AIP for Three Different Turbulence Model.....	36
Figure 3-13 Distortion Coefficient at AIP for Three Different Turbulence Model ...	37
Figure 3-14 Total Pressure Contours at AIP for Three Different Turbulence Models	38
Figure 4-1 Model.....	39
Figure 4-2 Dimensions of Fluid Domain	40
Figure 4-3 Boundary Conditions.....	40
Figure 4-4 Detailed View of Volume Grid	41
Figure 4-5 Corrected Mass Flow Rate Change for Different Static Pressures at AIP	42
Figure 4-6 Vortex Generators on Missile Surface	43
Figure 4-7 DC60 Values of Differently Oriented Vortex Generator Configurations	45
Figure 4-8 DC60 Difference with respect to INLET	46
Figure 4-9 DC60 Values of Vortex Generator Configurations with Different Heights	47
Figure 4-10 DC60 Difference with respect to INLET	48
Figure 4-11 DC60 Values of Vortex Generator Configurations with Different Lengths	50
Figure 4-12 DC60 Difference with respect to INLET	51
Figure 4-13 DC60 Values of Vortex Generator Configurations with Different Thicknesses	52
Figure 4-14 DC60 Difference with respect to INLET	53
Figure 4-15 DC60 Values of Vortex Generator Configurations with Different Positions	55
Figure 4-16 DC60 Difference with respect to INLET	56
Figure 4-17 DC60 Values of Vortex Generator Configurations with Different Positions	57
Figure 4-18 DC60 Difference with respect to INLET	58
Figure 4-19 DC60 Difference between VG2 and INLET	59
Figure 4-20 Average Total Pressure Distribution along Circumferential Direction at AIP	60

Figure 4-21 Total Pressure Contours of INLET and VG2 Configurations.....	61
Figure 4-22 Vectoral Representation of the Flow in Inlet for Configuration INLET	62
Figure 4-23 Vectoral Representation of the Flow in Inlet for Configuration VG2 ...	63

LIST OF TABLES

TABLES

Table 3-1 Fluid Properties.....	32
Table 4-1 Vortex Generator Models with Different Orientations.....	44
Table 4-2 Results of Vortex Generator Model with Different Orientations	45
Table 4-3 Vortex Generator Models with Different Heights	47
Table 4-4 Results of Vortex Generator Model with Different Heights.....	48
Table 4-5 Vortex Generator Models with Different Lengths.....	49
Table 4-6 Results of Vortex Generator Model with Different Lengths	50
Table 4-7 Vortex Generator Models with Different Thicknesses	52
Table 4-8 Results of Vortex Generator Model with Different Lengths	53
Table 4-9 Vortex Generator Models at Different Positions	54
Table 4-10 Results of Vortex Generator Model with Different Lengths	55
Table 4-11 Vortex Generator Models with Different Numbers	57
Table 4-12 Results of Vortex Generator Model with Different Numbers	58

CHAPTER 1

INTRODUCTION

A cruise missile is a guided missile which has almost constant velocity during its flight. The main purpose of cruise missile usage is to deliver large warheads for long distances. Modern cruise missiles are self-navigating and can operate at supersonic and high subsonic speeds. Various engine types have been used for the power supply such as solid-fueled rockets, turbojets, turbofans and ramjets. Considering high efficiency at high subsonic speeds, turbojet engines have been widely preferred during cruise missile design. Turbojet engine requires air to work and air must be supplied by inlets. Since cruise missiles have mostly axisymmetric body and air supply from nose is not preferred due to the concerns on the complexity of the system, S-duct inlet is commonly preferred. S-duct is a type of jet engine intake duct and a sample of S-duct inlet is represented in Figure 1-1.

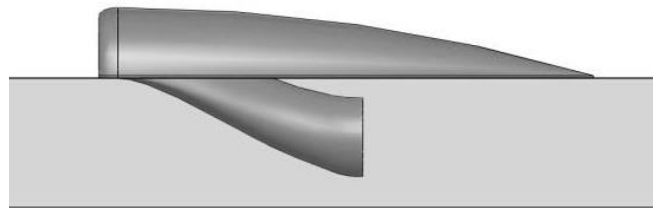


Figure 1-1 S-duct Inlet

The major challenge during S-duct inlet design is to ensure if the aircraft engine is properly supplied with air. Main purpose of an S-duct inlet is to translate the air from intake to the engine. Thus, shape of duct has a big role on the flow supplied to the engine. Engine of the aircraft requires air at subsonic speeds which is usually lower than the aircraft's flight speed. This requirement is fulfilled by the shape of the diffuser. It decelerates the flow velocity along its length. In other words, it converts

kinetic energy of the flow into potential energy. A desired S-duct inlet must efficiently decelerate the flow without the flow separation. Flow separation is obtained if the flow detaches from the wall [1]. Moreover, shorter duct is preferred to reduce drag, size and weight of the aircraft. However, shorter duct results in high degree of centerline curvature which leads to cross-stream pressure gradients. These gradients impart a transverse or cross flow velocity which is called secondary flow which is represented in Figure 1-2. The primary flow usually follows very closely to the flow pattern predicted by simple analytical techniques with an assumption of inviscid flow. A secondary flow is relatively minor flow superimposed on the primary flow. Secondary flow forming in terms of counter rotating vortices causes non-uniformity at engine face. Secondary flow moves the low profile fluid near the surface to the center of the duct. Streamwise pressure gradient can be formed by increasing of the cross sectional area. Combination of these effects causes flow separation which is the main reason of increased total pressure distortion (non-uniformity) and total pressure loss at the engine face [2].

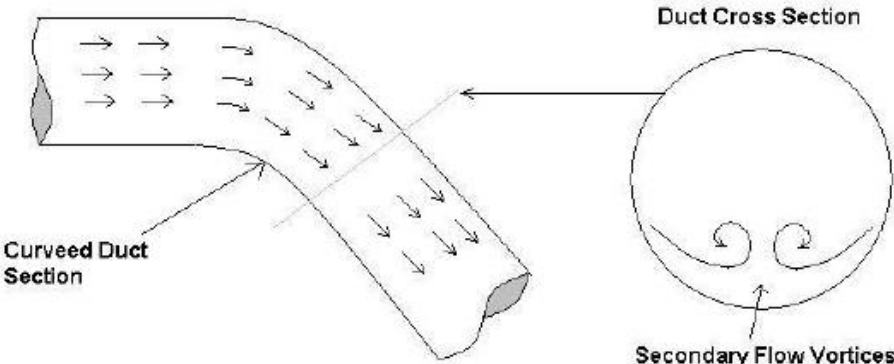


Figure 1-2 Representation of Secondary Flow Forming

Engine inlets must handle very challenging flows with strong adverse pressure gradients, boundary layer separation and strong secondary flows. The main reasons for forming this kind of flows are high diffusion over short duct lengths, turning of flow path, boundary layer ingestion, vortices and wake disturbances and shock-wave interactions. In order to eliminate or reduce these adverse effects, flow control devices are used since they control flow separation and engine face distortion by two

different ways. The first way is to mix low-momentum boundary layer flow with high momentum core flow. Second way is to use vortices for redirecting secondary flows. For both methods, main purpose of flow control device usage is to improve the performance of the inlet by decreasing pressure loss and face distortion at engine face [3].

1.1 Flow Control

In order to reduce adverse effects of secondary flow, several methods are used to control the flow and improve the flow uniformity at engine face. Flow control devices are used to direct high momentum flow into low momentum flow in order to increase energy of near-wall region [4]. However, this approach does not guarantee decrease of secondary flow and total pressure distortion.

Flow control can be classified in several ways. In this thesis, flow control is divided into two main parts which are closed and open flow controls.

1.1.1 Closed Loop Flow Control

The new generations of flow control devices are expected to improve inlet performance for several flight conditions. These devices are called as closed loop flow control devices which respond to changes in a feedback loop. In other words, flow control devices change their orientation with respect to upcoming flow in order to obtain improvement on the flow for different flight conditions. Closed loop flow control is still in the research and development stage at the moment and it can be more useful for inlet applications in future with innovation at sensing technology.

1.1.2 Open Loop Flow Control

In this flow control, there is no feedback loop contrary to closed loop flow control. It might involve different settings based on flight; however it is not with real time corrections. Since flow control devices do not receive any feedback, it is designed for limited flight conditions. However, despite of this weakness, they are widely used

because of their simplicity. In this thesis, several open loop flow control approaches are mentioned.

1.1.2.1 Vortex Generators

Vortex generators are usually small vane type sections placed on critical regions in order to reduce or eliminate effects of undesired flow like wake disturbances, upstream vortices, and upstream shock-wave boundary layer interactions [5]. Vortex generators are used in two different ways which are;

- To transport high momentum flow into low momentum boundary layer flow in order to reduce or eliminate boundary layer separation.
- To direct secondary flows [3].

A simple sketch of vortex generator vanes is shown in Figure 1-3.

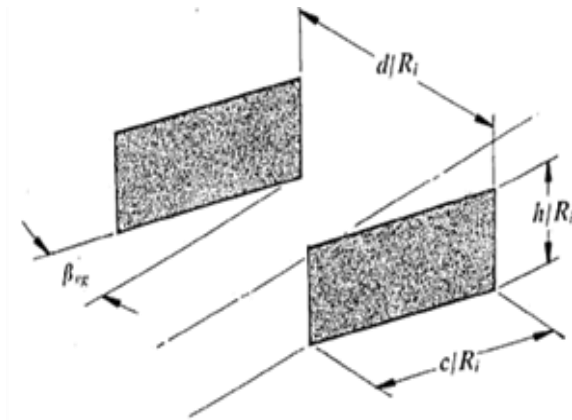


Figure 1-3 Vortex Generator Sample

1.1.2.2 Air Jets

In recent years, there has been a growing interest in air jet systems which are injecting high pressure air into the flow in order to create vortex. Studies have shown that air jets are usually easier to manufacture and more suitable for different flow

types comparing to vane type vortex generators. However, they are not effective as much as the vane type of vortex generators.

In a study by Jaw et al [6], experiments were performed with air jets in order to improve the inlet efficiency. Distortion was controlled with distortion screens and a hot air injection mechanism was used to simulate the inlet distortion. He used two different flow injection designs. First approach was to inject air from angled holes which are placed around a circumference. However, results were not satisfactory enough. In the second approach, holes were placed in an axially spaced row. The study revealed that amount of air to be injected significantly impacted the performance of the inlet. Excessive air injection led to secondary flow source development while insufficient air injection distortion did not reduce distortion enough. This experiment shows that optimization of flow control devices is essential for designers. Hamstra et al also compared the performances of air jets and vortex generator vanes. He concluded that vortex generator vanes had a greater performance than air jets [7].

1.2 Aim of the Thesis

Aim of the thesis is to improve the flow inside the duct to transfer it to engine with a desired quality. Thus, improvement in flow quality is essential since it directly affects engine performance. Otherwise, insufficient flow quality causes to distortion at engine face which decreases the operation range of the engine and reduces the life of the engines.

In the CFD analyses, FLUENT is used as solver and grids are generated by GAMBIT and TGRID. The method is validated with the test case Inlet-A [8] and the results are compared with experimental data. After validating CFD tools with the experimental data, analyses for the models with vortex generators are performed.

1.3 Literature Survey

The primary concerns of missile designers are to reduce cost and increase the possibility of stealth. Thus, integrating an inlet to the missile becomes a very important process. An inlet is used to decelerate the flow to the desired velocity for engine by maintaining high total pressure recovery and less flow distortion. Since an aircraft operates at many different flight regimes, aerodynamic design of an inlet is a challenging problem. Inlet shows completely different performances for changing flight regimes like take off, subsonic cruise and transonic maneuvering [5]. A good inlet must slow down the incoming flow efficiently for a wide range of flight conditions with minimum flow separation. By considering this feature of inlet, shorter ducts are also desired to design a good inlet because of space constraint on missile and lower contribution to missile weight. However, inlet bends give rise to streamline curvature. This curvature results in cross-stream pressure which produces secondary flow and secondary flow formation occurs within the boundary layer. These flows are in the form of counter rotating vortices at the duct exit. These vortices cause flow non-uniformity and flow separation at the inlet-engine interface [2].

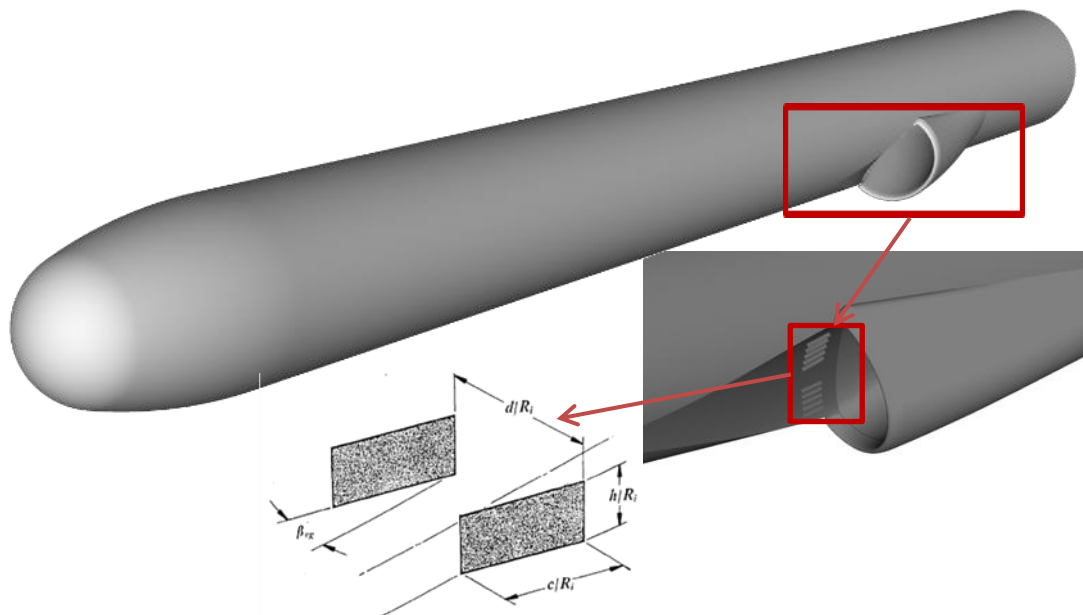


Figure 1-4 Air Intake and Vortex Generator [5]

Vortex generators are used to control the flow separation and inlet-engine interface distortion. There are various studies about vortex generators in order to improve inlet

performance over the interested flow region. In the design of vortex generators, several parameters such as dimensions and location of vortex generators are considered and optimized. Placing the vortex generators upstream of the inlet is one of the most commonly used methods in order to control the boundary layer separation. Depends on the problem, some designers prefer to locate vortex generators inside the surface of the inlet duct. Common specific properties of the vortex generators are that they are small vanes and placed with an angle to the upcoming flow. They are typically in the form of thin rectangular or triangular vanes and they are sized considering the boundary layer thickness. A sample of vortex generators is illustrated in Figure 1-4.

According to Bernhard H. Anderson [5], vortex generators can be divided into two basic different configurations which are shown in Figure 1-5. The difference between these two configurations is the inclination of the vortex generators to the upstream flow. In the first configuration, all vortex generators are inclined at the same angle. On the other hand, in the second configuration, half of vortex generators are inclined by positive angle of attack and the others by a negative angle of attack. The former one is called co-rotating configuration and created vortices rotate in the same direction. The latter one is called counter-rotating configuration and created vortices are counter-rotating. Co-rotating configurations are more effective within S-duct inlet configurations especially in the boundary layer region. Counter-rotating configurations are effective in reducing flow separation. If these two configurations are compared, counter-rotating configuration has disadvantages like;

- Induced vortices causes lift off the duct surface
- Higher pressure recovery loss
- Higher total pressure distortion.

Their common feature is to obtain better performance at engine face by decreasing the engine face distortion.

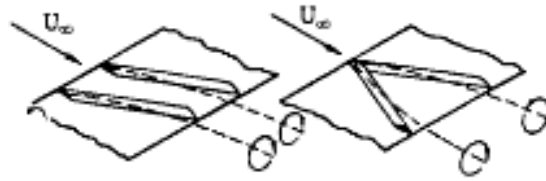


Figure 1-5 Co-rotating and Counter-Rotating Vortex Generators [9]

Flow control devices for inlets have been studied since late 1940s. Taylor [10] worked on vortex generator vanes in order to increase energy of boundary layer. He aimed to prevent flow separation. Percy and Stuart [11] and Valentine and Carrol [12] continued Taylor's investigation of flow control devices into the 1950s. Their goals were usually to prevent flow separation based on two-dimensional boundary layer concept. Percy designed many successful and unsuccessful configurations such as counter rotating and co-rotating vortex generators with different geometries. As a result, vortex generator vanes did not work efficiently for the cases with regions of large secondary flow.

Kaldschmidt, Syltebo, and Ting [13] proved that one could recreate the development of the secondary flow by improving inlet-engine interface distortion. They created a new approach which moved attention away from separation control to a global manipulation of the secondary inlet flow. This new approach had some requirements like solving the three-dimensional viscous flow equations. Anderson and Levy [14] demonstrated how to design passive vortex generator devices by solving three-dimensional viscous flow equations.

Reichert and Wendt tested parameters such as vortex generator height, location of vortex generator and their spacing. They concluded that varying the spacing of the vortex generators along the circumferential distance has almost no effect on separation. On the other hand, longitudinal spacing is very critical. Vortex generators are working well when they are placed upstream of the point of separation. Placing them close to the separation point or downstream of the point of separation has a little effect on the flow. In addition, increasing height of vortex generator reduces the distortion level. However, pressure recovery is adversely affected by increasing height of vortex generator. Optimum height of vortex generators is around boundary

layer thickness. Decreasing space between vanes reduces the separation area, decrease total pressure recovery and increase the distortion [15].

Reichert and Wendt also performed experiments of vortex generators inside the duct which create vortices in opposite direction to the naturally formed vortices. They concluded that the flow should be carefully analyzed and vortex generators were placed at precise locations in this approach. By this approach, optimum orientation of the vanes can be easily found; however manufacturing of the duct is difficult. In addition, breaking of vanes in the flight can damage the engine. In the end, the flow control devices eliminated the separation, increased pressure recovery and decreased distortion at engine face [16].

Even though there have been many important researches on inlet flow control, insufficient researches on flow control devices are available in the literature. Anabtawi, Blackwelder, Liebeck, and Lissaman [17] performed first experiments for an S-shaped duct for low Mach numbers. The experiment results showed that passive flow control devices improved the inlet-engine interface distortion at operation conditions. Gorton, Owens, Jenkins, Allan and Schurster [18] rebuilt up this research by using active flow control jets with passive flow control devices. This experiment could demonstrate that jets could be preferred to reduce distortion. It also provided a database for OVERFLOW [19] which is a NASA developed Reynolds-averaged Navier-Stokes (RANS) flow solver. This flow solver was used to guess jet actuator locations which were used in modification of the baseline inlet model. Allan, Owens, and Lind performed a Design of Experiment (DOE) for a vortex generator configuration to be tested in transonic regime [20]. Today, DOE is used to build a response surface model for an inlet flow control design. Several design factors and optimization of the flow control design are taking into account in order to minimize flow distortion.

Lin performed an exploratory study that he tried to control flow separation by using vortex generators. Vortex generator devices move high momentum fluid into the boundary layer. As a result, boundary layer becomes thinner and increases its resistance to adverse pressure gradients which lead to flow separation. Lin has found

that the vortex generator devices whose height is shorter than boundary layer height are more effective because their velocity gradient is higher. They are called as ‘submerged’ vortex generators. [2]

More recent studies of Lin revealed that so called boundary layer vortex generators (SBVGs) are working more effective comparing to conventional bigger vortex generators with height almost equals to local boundary layer thickness. SBVGs are smaller devices with height of $0.1 < h_{VG}/\delta_{99} < 0.5$ where h_{VG} is the height of SBVG vanes height and δ_{99} refers to local boundary layer thickness. By this way, SBVG vanes mix the flow only within the boundary layer.

There are some other vortex generators which are different from the conventional vortex generators. Wheeler [21] and Kuethe [22] designed two examples of them. Their common property is that they are both fully submerged within the boundary layer. Wheeler type vanes are wedge-shaped bodies of triangular planform. They create counter-rotating spiral vortices. Kuethe vanes are wavy-wall type and the wave crests lie obliquely to the external flow. Wheeler and Kuethe type vanes are represented in Figure 1-6.

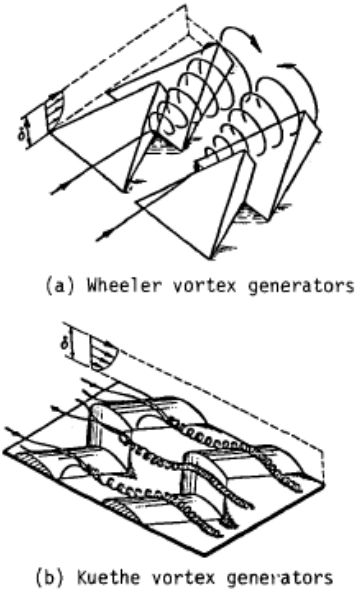


Figure 1-6 (a) Wheeler Vortex Generators, (b) Kuethe Vortex Generators [9]

Akshoy Ranjan Paul [2] was influenced by Lin and performed an experiment with an S-shaped diffuser which has rectangular cross section. He aimed to see the effects of the corners on exit flow pattern. He used ‘fishtail’ type of vortex generators at different locations and in changing numbers in order to control secondary flow. Fishtail type of vortex generator is shown in Figure 1-7. They have observed that locations of vortex generators were more effective than the number of vortex generators.

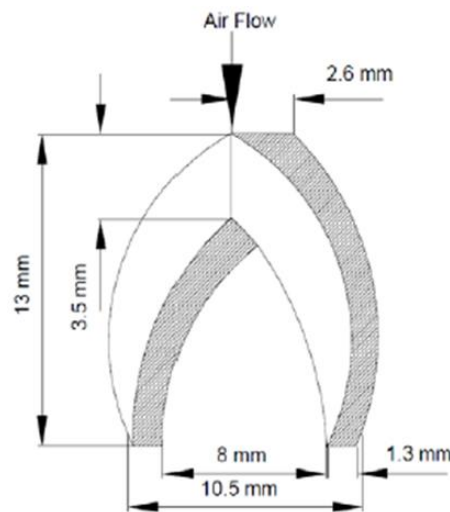


Figure 1-7 Fishtail Shaped Submerged Vortex Generator [2]

Computational fluid dynamics (CFD) is used to simulate inlet flows and design inlets to obtain better performance. Since vortex generators are used to improve the inlet performance, vortex generators should be included in these simulations. However, designing different vortex generator combinations is neither practicable nor desirable. For each configuration, computational grids must be generated. In addition, computation of the solution must be performed. This process is both time and effort consuming. Therefore, NASA Glenn developed Wendt empirical vortex generator model and integrated it into Wind-US Navier-Stokes code. Julianne C. Dudek explained the Wendt vane-type vortex generator model, its integration into the Wind-US code and usage guidelines. [3].

CHAPTER 2

METHODOLOGY

In this chapter, governing equations for fluid flow will be introduced. Then discretization techniques and boundary conditions will be discussed. In addition, calculations of inlet performance parameters are explained.

2.1 Governing Equations

In this study, compressible and steady form of Reynolds-Averaged Navier-Stokes (RANS) equations are used. Several turbulence models are also examined.

2.1.1 Fluid Modeling

Solving Navier-Stokes equations require high computer performance and time. Recent computer technology is insufficient to solve complex Navier-Stokes equations. Therefore, it makes more important to use simplified Navier-Stokes equations. Thus, governing equations of steady and compressible Reynolds-Averaged Navier-Stokes equations, which take into account the viscous effects, are used to model fluid flow. The equation for conservation of mass, momentum and energy can be written as follows:

$$\frac{\partial \rho}{\partial t} + \nabla \cdot (\rho \vec{V}) = 0 \quad (2.1)$$

$$\rho \frac{D\vec{V}}{Dt} = -\nabla p + \nabla \cdot (\tau_{ij}) + \rho \vec{g} \quad (2.2)$$

$$\rho \frac{Dh}{Dt} = \frac{Dp}{Dt} + \nabla \cdot (k\nabla T) + \tau_{ij} \frac{\partial u_i}{\partial x_j} \quad (2.3)$$

The stress tensor τ_{ij} is given as;

$$\tau_{ij} = \mu \left(\frac{\partial u_i}{\partial x_j} + \frac{\partial u_j}{\partial x_{ji}} \right) + \delta_{ij} \lambda \nabla \cdot \vec{v} \quad (2.4)$$

Navier-Stokes equations are a system of five equations with seven unknowns which are ρ , u , v , w , E , p and T . Thus, two more equations are required in order to solve the problem. In the analyses, the flow is set as compressible. Therefore, air is assumed to be ideal gas and the equation of state is stated as [23];

$$p = \rho RT \quad (2.5)$$

Moreover, dynamic viscosity term μ is calculated by using Sutherland's law [23].

$$\mu = \frac{1.45T^{\frac{3}{4}}}{T + 110} 10^{-6} \quad (2.6)$$

Stagnation state properties should also be calculated in order to characterize the compressible flow. For constant C_p , following equations are used.

$$\frac{p_o}{p} = \left(1 + \frac{\gamma - 1}{2} M^2 \right)^{\gamma/(\gamma-1)} \quad (2.7)$$

$$\frac{T_o}{T} = 1 + \frac{\gamma - 1}{2} M^2 \quad (2.8)$$

2.2 Numerical Tool and Discretization

FLUENT which is a commercial program is used as the CFD solver in this study. [24].

2.2.1 Grid Generation

The grid for the CFD solver is created by using GAMBIT. TGRID is another commercial program which is used for boundary layer formation. The following procedure is followed during grid generation.

- Drawing solid model at GAMBIT,
- Generating surface grid with triangular elements,
- Exporting mesh to TGRID in order to form boundary layer,
- Exporting mesh with boundary layer to GAMBIT to create volume grid with tetrahedral elements,
- Exporting volume mesh to FLUENT.

2.2.2 Flow Solver

In this thesis, the density-based solver which is a numerical method to solve the flow is used. The density-based solver solves the continuity, momentum and energy and species of transport equations coupled together. Equations for additional scalars are solved afterward since the equations are non-linear and a couple of iterations of the loops must be carried out. The following steps are performed:

- Update fluid properties based on current solution,
- Solve the Navier-Stokes equations (continuity, momentum and energy) simultaneously,
- If it is necessary, solve equations for scalars like radiation or turbulence by using the updated values of other variables,
- Control if the solution is converged.

Flow chart of the working procedure of density-based solution method is presented in Figure 2-1.

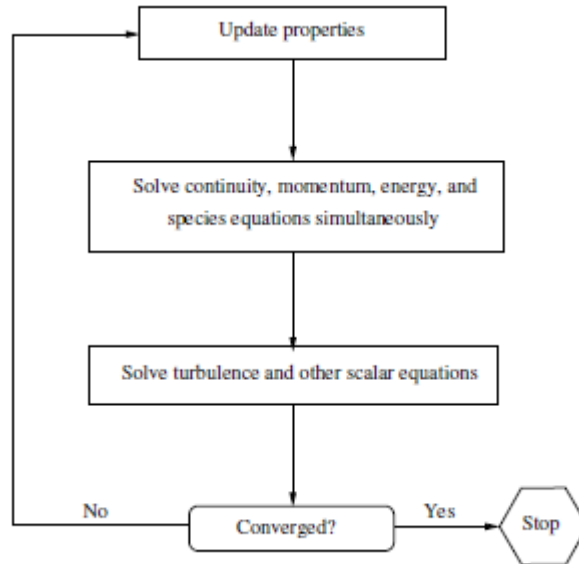


Figure 2-1 Overview of the Density-Based Solution Method

Governing equations are linearized in a form of “implicit” with respect to the interested dependent variables. Both existing and unknown variables at neighboring cells are used in the relation which is used to compute the unknown values in each cell. Thus, each unknown variables will be in several equations in the system and these equations must be solved simultaneously.

2.2.3 Discretization

FLUENT converts a general transport equation to algebraic equation numerically in order to solve it numerically by using a control-volume based technique. This technique integrates the transport equation for each control volume and yields a discrete equation which expresses the conservation laws. Integral form of governing equations for an arbitrary scalar ϕ is represented in the following form.

$$\int_V \frac{\partial \rho \phi}{\partial t} dV + \oint \rho \phi \vec{v} \cdot d\vec{A} = \oint \Gamma_\phi \nabla \phi \cdot d\vec{A} + \int_V S_\phi dV \quad (2.9)$$

ρ , \vec{v} and \vec{A} are density, velocity vector and surface vector area respectively. Gradient of ϕ and source of ϕ per unit volume are shown as $\nabla\phi$ and S_ϕ sequentially. The above equation is in the integral form for an arbitrary control volume V . This formula is used for each control volume/cell in the domain. A control volume used to illustrate discretization is represented in Figure 2-2.

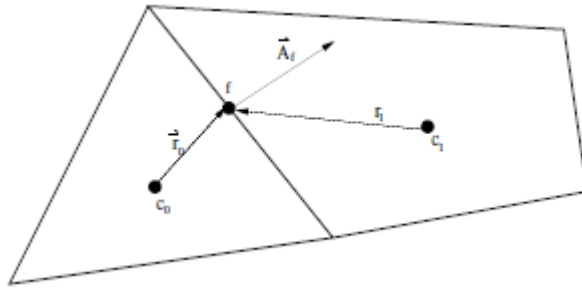


Figure 2-2 An Example of Control Volume Used for Discretization of a Scalar Transport Equation

Integral form of governing equation is discretized below. N_{faces} is the number of faces of the control volume. ϕ_f is the value of ϕ which is convected through the face f .

$$\frac{\partial \rho \phi}{\partial t} V + \sum_f^{N_{\text{faces}}} \rho_f \vec{v}_f \phi_f \cdot \vec{A}_f = \sum_f^{N_{\text{faces}}} \Gamma_f \nabla \phi_f \cdot \vec{A}_f + S_\phi V \quad (2.10)$$

2.2.4 Turbulence Modeling

Fluctuating velocity fields determines the characteristic of the turbulent flow. Transported quantities are mixed by these fluctuations and they also fluctuate. Fluctuations which are with small scale and high frequency take huge time and resources to solve. Thus, exact governing equations can be simplified by averaging time and ensemble. By this way, modified set of equations which need less computational power to solve are obtained. To note that, these modified set of equations include a couple of new unknown terms. Therefore, turbulence models are required to determine these variables in terms of known quantities.

There are several numerical methods for turbulence modeling which are represented in Figure 2-3. The most common ones are Reynolds Averaged Navier-Stokes (RANS), Large Eddy Simulation (LES) and Direct Numerical Simulation (DNS). There is no single turbulence model which is accepted to be superior for all class of problems. Therefore, choosing turbulence model is based on physics encompassed in the flow, the established practice of the problem, accuracy requirement, available computational tools, and amount of time. In order to decide best turbulence model for a problem, it is better to know capabilities and limitations of the turbulence models.

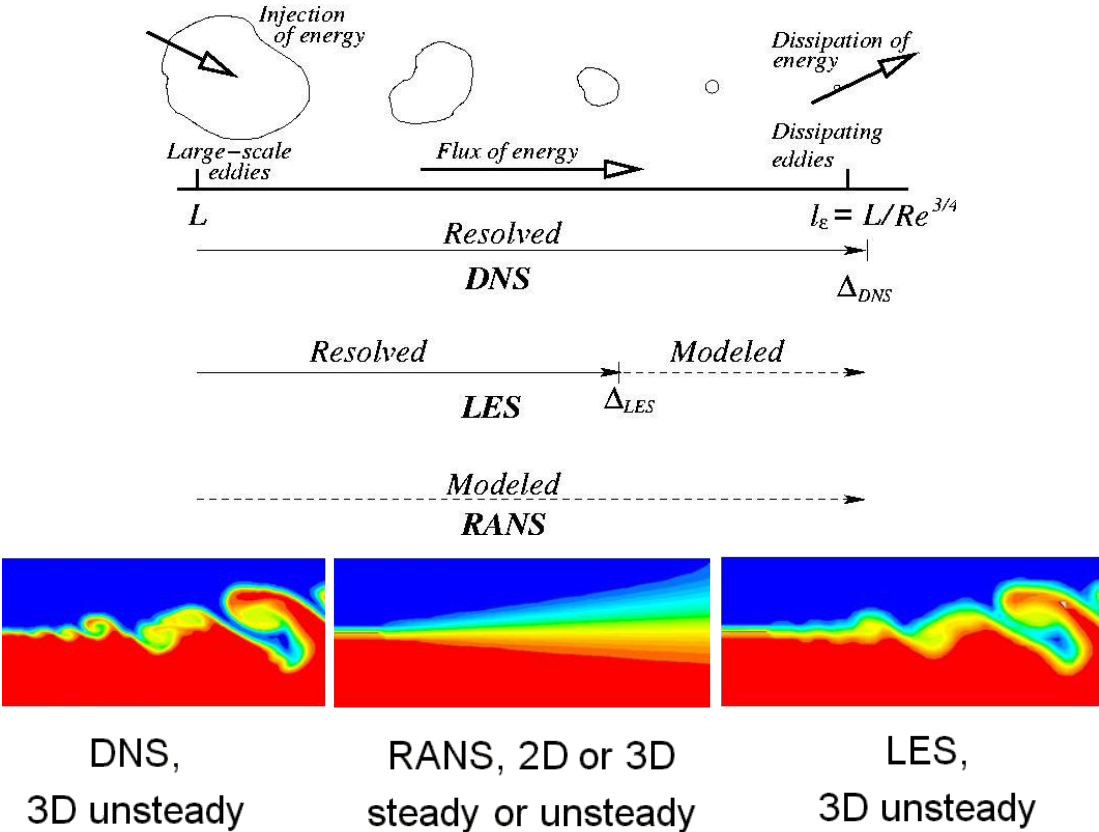


Figure 2-3 Numerical Methods for Turbulence Modeling

All scales of eddies are solved in DNS method. Small time and length scales are essential for this approach. Solution domain must contain very fine mesh in order to capture flow characteristics. DNS is computationally expensive such that for a diffuser analysis with $Re=10000$, 220 million grid nodes are required. LES solves time dependent filtered Navier-Stokes equations by explicit methods. Only small

eddies are modeled. It requires less grid points comparing to DNS. However, it is still computationally costly. The most commonly used method for practical fluid problems is the RANS method. Average flow variables are used in calculations. RANS method dramatically reduces the required computational work and time. Therefore, it is widely preferred for practical engineering problems. In RANS method, the solution variables in the exact Navier-Stokes equations are separated into ensemble or time averaged and fluctuating components. For instance, velocity components are given as:

$$u_i = \bar{u}_i + u_i' \quad (2.11)$$

\bar{u}_i and u_i' are the mean and fluctuating velocity component respectively. In same manner, a general formula for other scalar quantities can be written as;

$$\phi = \bar{\phi} + \phi' \quad (2.12)$$

Substituting the unknown flow variable into the instantaneous continuity and momentum equations and averaging time will give ensemble-averaged momentum equations which is written in Cartesian tensor form and represented below.

$$\frac{\partial \rho}{\partial t} + \frac{\partial}{\partial x_i} (\rho u_i) = 0 \quad (2.13)$$

$$\begin{aligned} \frac{\partial}{\partial t} (\rho u_i) + \frac{\partial}{\partial x_j} (\rho u_i u_j) = & \frac{\partial}{\partial x_i} + \frac{\partial}{\partial x_j} \left[\mu \left(\frac{\partial u_i}{\partial x_j} + \frac{\partial u_j}{\partial x_i} - \frac{2}{3} \delta_{ij} \frac{\partial u_l}{\partial x_l} \right) \right] \\ & + \frac{\partial}{\partial x_j} (-\overline{\rho u_i' u_j'}) \end{aligned} \quad (2.14)$$

They are called RANS equations. Only difference from the general form is that solution variables are time or ensemble averaged values. Additional term $-\overline{\rho u_i' u_j'}$ arises and determines the effects of turbulence. This term is called Reynolds stress and must be modeled.

Boussinesq hypothesis is the mostly used method in order to relate Reynolds stress term to the mean velocity gradients.

$$-\rho \overline{u_i' u_j'} = \mu_t \left(\frac{\partial u_i}{\partial x_j} + \frac{\partial u_j}{\partial x_i} \right) - \frac{2}{3} \left(\rho k + \mu_t \frac{\partial u_k}{\partial x_k} \right) \delta_{ij} \quad (2.15)$$

k- ϵ , k- ω and Spalart-Allmaras models use the Boussinesq hypothesis since its advantage of low computational cost requirement. μ_t and k are turbulent viscosity and turbulent kinetic energy respectively. Spalart-Allmaras solves one additional transport equation. On the other hand, k- ϵ and k- ω models solve two additional transport equations. For k- ϵ model, μ_t is computed as a function of k and ϵ . In the case of k- ω model, k and ω are used in order to compute μ_t . ϵ is the turbulence dissipation rate and ω is the specific dissipation rate.

In this thesis, only RANS turbulence models are used since other methods require more time and impractical for industrial applications.

2.2.4.1 Spalart-Allmaras Model

The Spalart-Allmaras model is a one-equation RANS model which solves additional transport equation for the kinematic turbulent viscosity. It uses rotational rate tensor in order to calculate turbulence viscosity. Therefore, it gives relatively good results for the flows with vortices. The Spalart-Allmaras method gives successful results for low separated flows, wall bounded flows and flows with recirculation. On the other hand, it gives unsatisfactory results for the flows with high separation, free shear and simple decaying turbulence.

2.2.4.2 Realizable k- ϵ Model

Realizable k- ϵ model is the modified version of Standard k- ϵ model which includes a new formulation to calculate turbulent viscosity. The dissipation rate ϵ is obtained from an exact equation for the transport of the mean-square vorticity fluctuation. It predicts the spreading rate of planar and round jets accurately. In addition, it gives

satisfactory performance for flows including rotation, boundary layers with strong adverse pressure gradients, separation and recirculation.

2.2.4.3 Standard k- ω Model

Standard k- ω model is a two-equation RANS model which based on transport equations for k (turbulent kinetic energy) and ω (specific dissipation rate). Turbulence viscosity is calculated by k and ω values.

$$\mu_t = \alpha \frac{\rho k}{\omega} \quad (2.16)$$

k- ω method is superior over k- ϵ method for low Reynolds flows. Thus, it can be used for near-wall region without any modification. In addition, it has a better accuracy for free shear flows. It is usually preferred by the problems which include wake and mixing layers.

2.2.4.4 Near-Wall Treatment

Since the walls are the main reason of vorticity and turbulence formation, numerical solutions are affected by the near wall modelling to a great degree. In the near-wall region, solution variables have large gradients. Thus, the more accurate representation of the flow near the wall is performed, the more successful predictions of wall bounded turbulent flows are determined.

The near-wall region separated into three layers which are viscous sublayer, fully-turbulent layer and buffer layer and they are shown in Figure 2-4. Viscous sublayer is the inner layer in which the flow is almost laminar and the momentum and heat or mass transfer is mostly affected by viscosity. The outer layer is called as fully-turbulent layer. Turbulence has significant impact in this region. The layer between viscous sublayer and fully-turbulent flow is buffer layer. The importance of molecular viscosity and turbulence is almost same in this region.

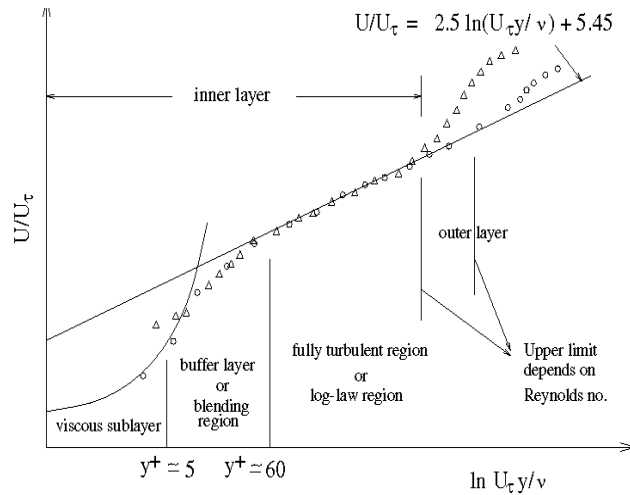


Figure 2-4 The Near-Wall Region with Separated Layers

Near-wall region is modeled by two different ways. The first model is called wall function approach. In the first approach, viscous sublayer and buffer region are not directly solved. Instead, semi empirical formulas which are wall functions are used to connect the wall and the fully-turbulent region. The second method is near-wall model approach. Turbulence models are able to solve viscous areas with a mesh including the viscous sublayer. Wall function approach is preferable for high Reynolds number flows, since the solution variables that change rapidly are not necessary to be solved. It is computationally economical and it gives satisfactory results. On the other hand, the wall function approach does not give satisfactory results for low Reynolds number flows, since the assumptions used in wall functions are not valid for low Reynolds number flows. Near-wall region models are compared in Figure 2-5.

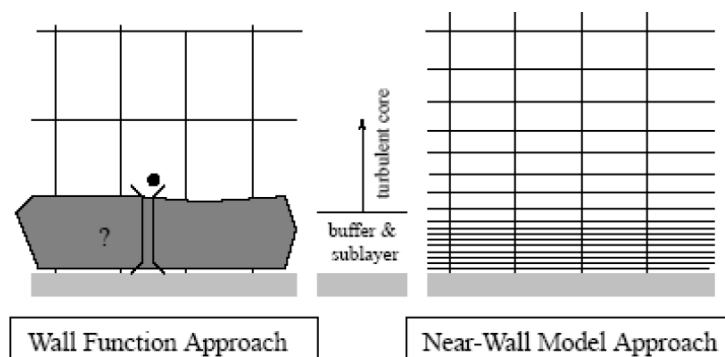


Figure 2-5 Near-Wall Region Models (a) Wall Function Approach, (b) Near-Wall Model Approach

For wall-function approach, height of first cell must be lower than boundary layer thickness and y^+ must be lower than 100. y^+ is a function of Reynolds number and kinematic viscosity. It is a non-dimensional parameter which determines the distance between the wall boundary condition surface and the first adjacent cell face. In the analyses, enhanced wall treatment is commonly used because of its satisfactory performance around wall. y^+ value must be around 1 in order to capture the sudden changes in gradients around the wall.

$$y^+ = \frac{yu_\tau}{\nu} \quad (2.17)$$

$$u_\tau = \sqrt{\frac{\tau_w}{\rho}} = U \sqrt{\frac{\bar{c}_f}{2}} \quad (2.18)$$

$$\frac{\bar{c}_f}{2} = 0.037Re_L^{-0.2} \quad (2.19)$$

u_τ , U , and \bar{c}_f are friction velocity, free stream velocity, and skin friction coefficient respectively.

2.3 Inlet Performance Parameters

Inlet parameters such as mass flow rate, pressure recovery and distortion coefficient mainly determine the performance of inlet. Therefore, it is important to understand what these parameters mean and the concepts behind them.

2.3.1 Mass Flow Rate

Mass flow rate is the mass of air which passes through Aerodynamic Interface Plane (AIP) per unit of time. This parameter varies with density and speed of air, and area of AIP. AIP section is represented in Figure 2-6

$$\dot{m} = \rho \cdot V \cdot A_{AIP} \quad (2.20)$$

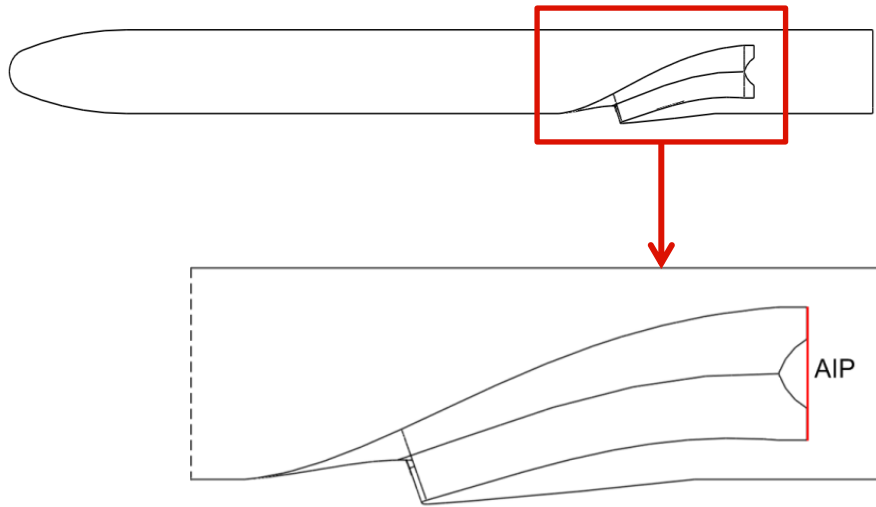


Figure 2-6 AIP section

2.3.2 Corrected Mass Flow Rate

A general term corrected mass flow rate is desired to compare mass flow rate for different flight conditions. In this formula, total temperature and pressure values are converted into non-dimensional values with sea level total temperature and pressure. Corrected mass flow rate is formulated in the following form;

$$\dot{m}_{\text{corrected}} = \frac{\dot{m}(\sqrt{T_{t,AIP}/T_{\text{sea level}}})}{P_{t,AIP}/P_{\text{sea level}}} \quad (2.21)$$

2.3.3 Pressure Recovery

Inlet performance is determined in terms of pressure recovery and distortion. Pressure recovery is the ratio of average total pressure at AIP to freestream total pressure. It is one of the most important parameter which determines inlet performance. To design an inlet with satisfactory performance, maximum total pressure recovery is desired for one or more operating conditions.

$$PR = \frac{P_{t,avg,AIP}}{P_{t,\infty}}, \quad 0 \leq PR \leq 1 \quad (2.22)$$

2.3.4 Distortion Coefficient

Total pressure variation on the engine face is defined as flow distortion. Flow distortion indicates if the flow is uniform or non-uniform. Inlet distortion is not desired since it can reduce surge margin and limit maneuverability of the missile. Even though inlet distortion occurs in the inlet, it mostly affects the response of engine. Since it is impractical at the engine face to measure distortion, inlet designers agreed to use AIP which is forward of the compressor face.

The mostly used quantitative distortion descriptor in the literature is simply;

$$DC_{\theta} = [P_{T,max} - P_{T,min}] / q_{ave} \quad (2.23)$$

Theta values can vary with engine design. Commonly used theta values are 60°, 90° and 120° [5]. For the inlets used in this thesis, the distortion analyses are performed for the theta values of 60° because of the engine requirements.

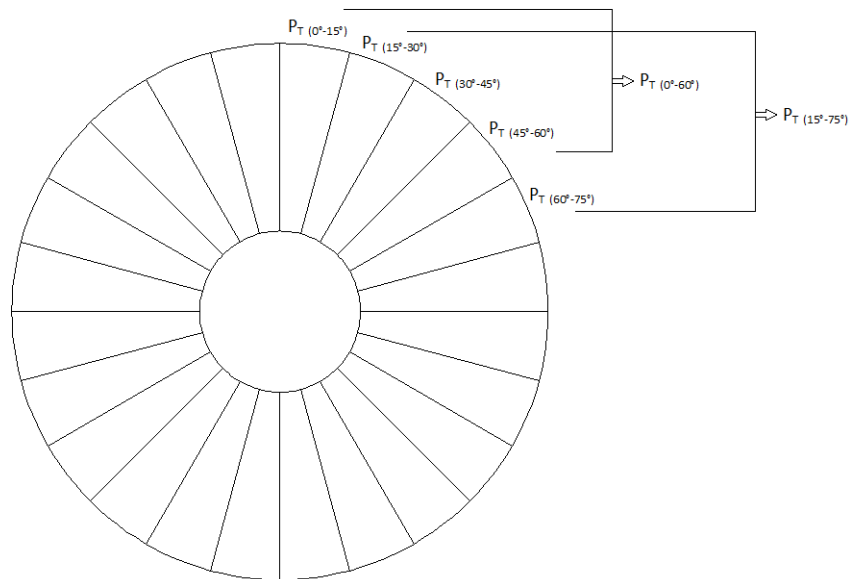


Figure 2-7 15° and 60° Pieces on AIP

To calculate DC60 value, the first step is to divide AIP into 24 equal pieces which is represented in Figure 2-7. Each piece corresponds to 15° slices. Area weighted average of total pressure of each slices are obtained and represented such as $P_{T(0^{\circ}-15^{\circ})}$, $P_{T(15^{\circ}-30^{\circ})}$, ..., $P_{T(345^{\circ}-360^{\circ})}$. The second step is to calculate area weighted average of total pressure of each 60° slices ($P_{T(0^{\circ}-60^{\circ})}$, $P_{T(15^{\circ}-75^{\circ})}$, ..., $P_{T(345^{\circ}-45^{\circ})}$) which are shown in Figure 2-8. $P_{T,min}$ is the minimum average total pressure of 60° slices. $P_{T,ave}$ is the average of weighted average of total pressure of 15° slices. Finally, DC60 is calculated as;

$$DC60 = \text{abs}[P_{T,min} - P_{T,ave}] / q_{AIP} \tag{2.24}$$

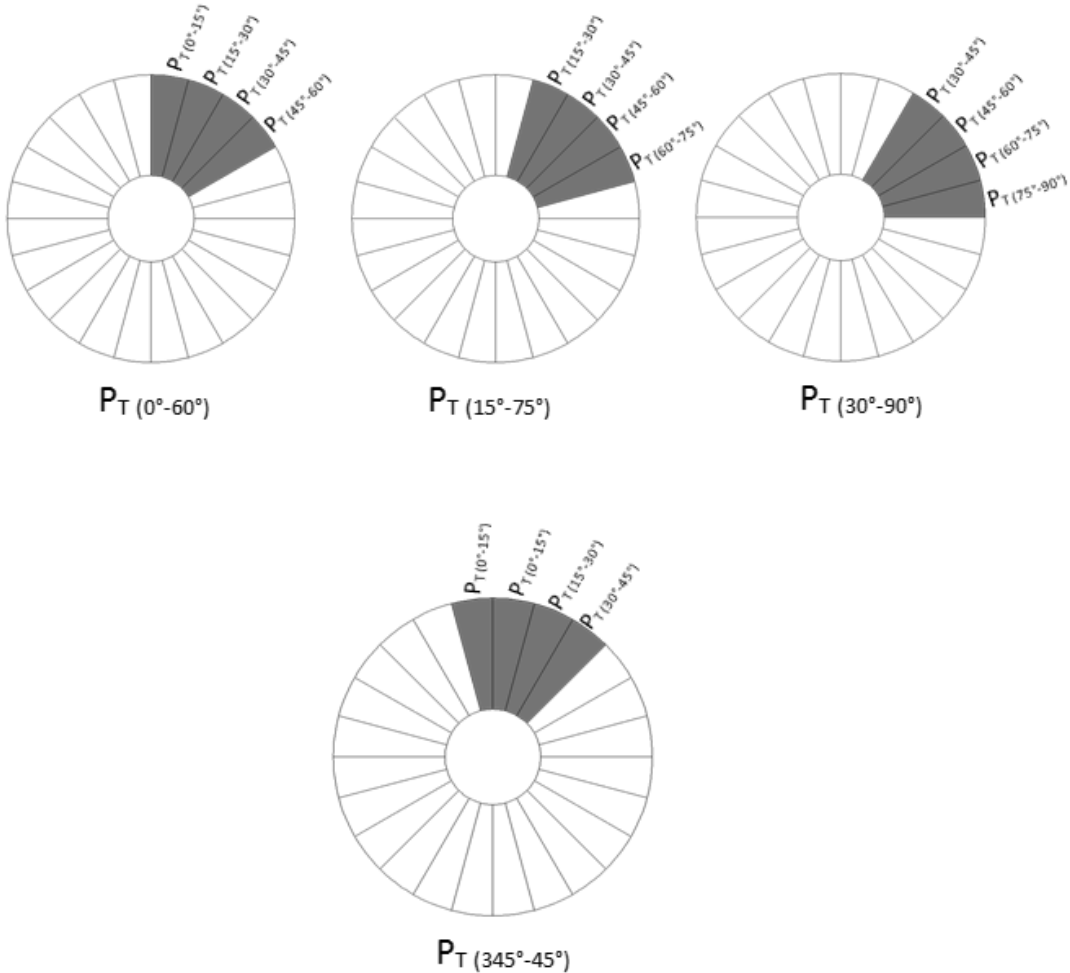


Figure 2-8 Calculation of 60° Pieces on AIP

CHAPTER 3

VALIDATION OF AERODYNAMIC MODEL

Since CFD is less costly and faster than performing experiments, CFD is highly preferred for industrial applications. However, its reliability and accuracy must to be examined for specific problems so results of CFD analyses must be validated with similar experiment results. Since the most interested region of the analyses is inlet part of the missile in this thesis, another inlet which has experimental results in the literature is modeled and solved with CFD tools. In this section, CFD results of Inlet-A [25] are compared with wind tunnel test results. Aerodynamic performance analyses for Inlet-A test case are conducted at National Aeronautics and Space Administration (NASA) Langley Research Center 0.3-Meter Transonic Cryogenic Tunnel. Inlet-A is designed by the Boeing Company for Blended-Wing-Body (BWB) transport and military aircraft applications.

3.1 Inlet-A Test Case

The test case model Inlet-A is an S-duct inlet configuration and represented in Figure 3-1.

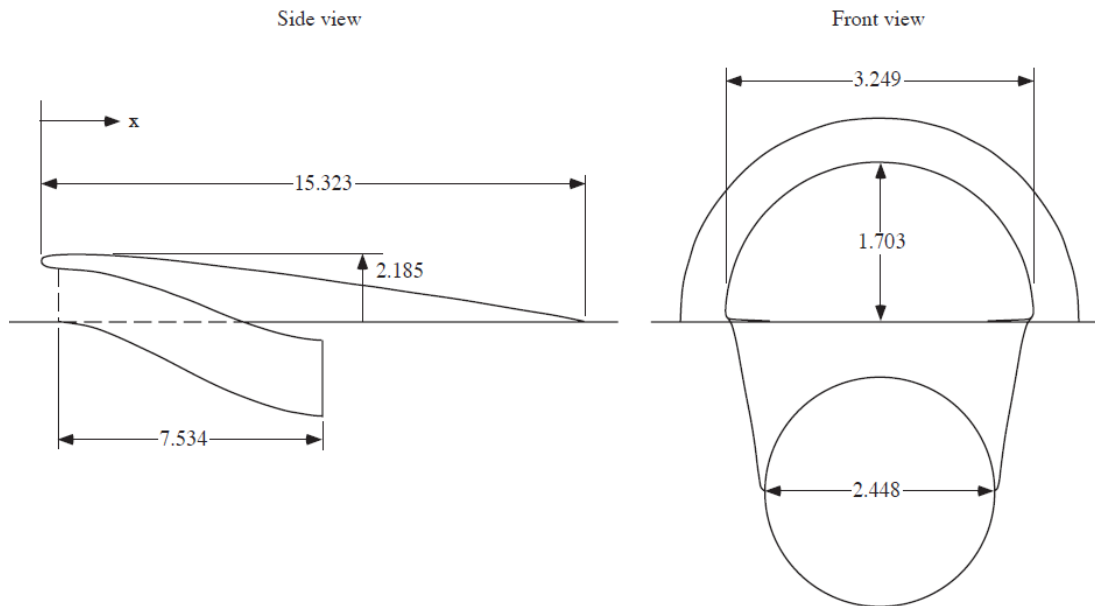


Figure 3-1 Geometry of Inlet-A [26]

Inlet A was integrated into a new tunnel sidewall. Photos of the inlet attached to the sidewall are given in Figure 3-2. Since the model was mounted to the sidewall, angle of attack (α) and sideslip angle (β) are set to zero degrees. The inlet laid down into the wall and connected to wind-tunnel plenum. At the exit of the inlet, the flow entered to a section with full of instruments. At this section, pressure recovery and distortion data at the Aerodynamic Interface Plane (AIP) were collected. Inlet flow was performed by pressure difference between tunnel total pressure and atmospheric pressure.



Figure 3-2 Photograph of Inlet Model Mounted on Tunnel Sidewall. [8]

There were 74 static pressure orifices at the AIP. 60 of them were located at upper and lower wall centerlines and remaining orifices were put on each sidewall. Locations of static pressure orifices are represented in Figure 3-3. An equal area-weighted 40-probe total pressure rake with 8 arms and 5 instrument rings in AIP were used to get inlet pressure recovery and distortion data. Probes can be seen in Figure 3-4.

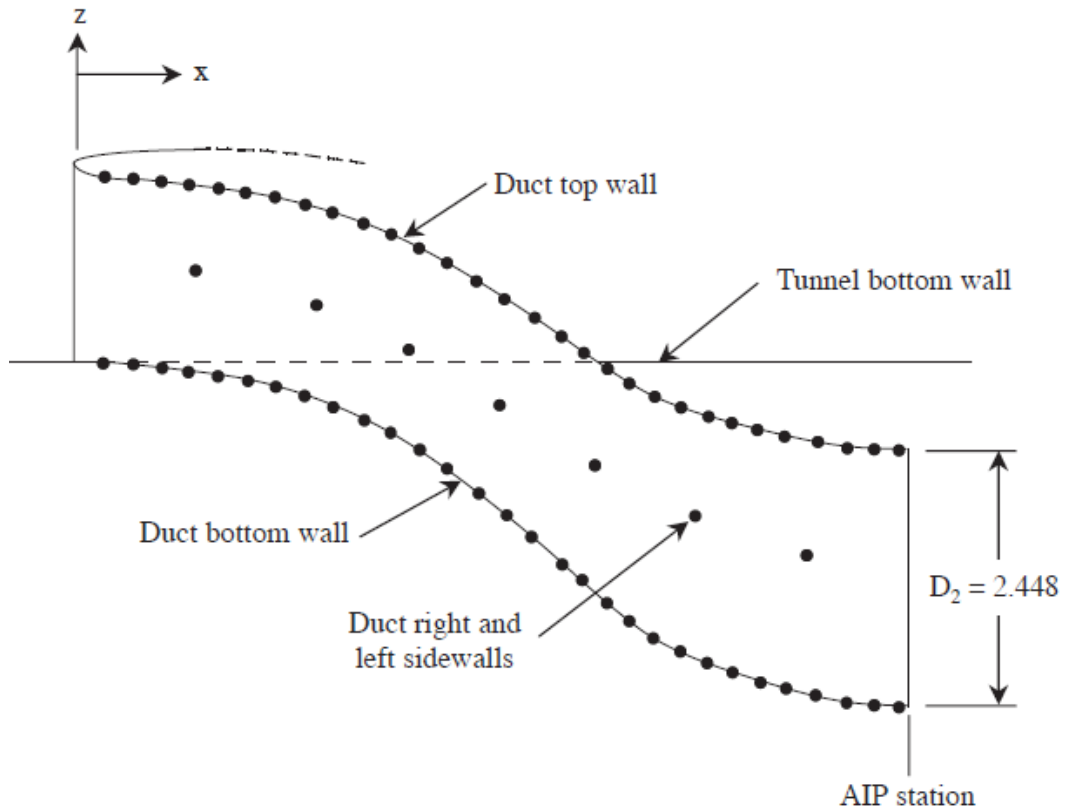


Figure 3-3 Locations of Static Pressure Orifices on Inlet Walls [26]

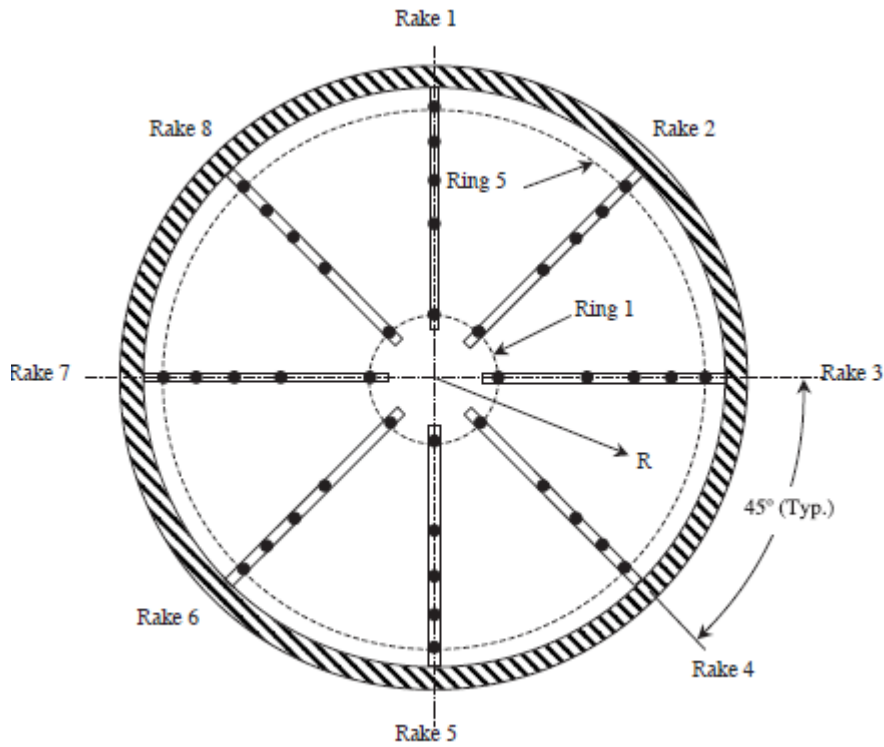


Figure 3-4 Probes at AIP [26]

3.2 Numerical Simulation

The numerical solution of the Inlet-A were performed for a steady, compressible and turbulent flow by using FLUENT.

3.2.1 Solid Model

The model is created by using the software GAMBIT. Tunnel sidewall is also modeled so that the inlet model mounted flush with the wall. The created model is shown in Figure 3-5.

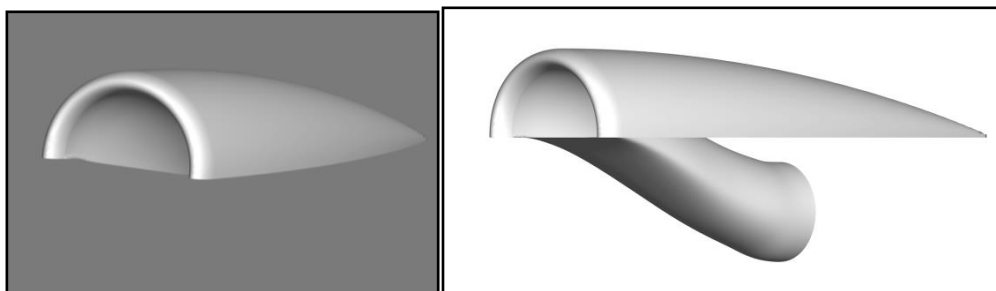


Figure 3-5 Solid Model of Inlet-A

A flow domain is created surrounding the inlet. The inlet is placed at a distance of 2 times inlet diameter ($2D_{inlet}$) above the bottom of a rectangular prism. Upstream length is $17.5D_{inlet}$ while the downstream length is equal to $16D_{inlet}$. Width of the flow domain is $22D_{inlet}$. Dimensions of rectangular prism fluid domain with $22D_{inlet}$ depth are given in Figure 3-6 in which dimensions are given in the format of inlet diameter.

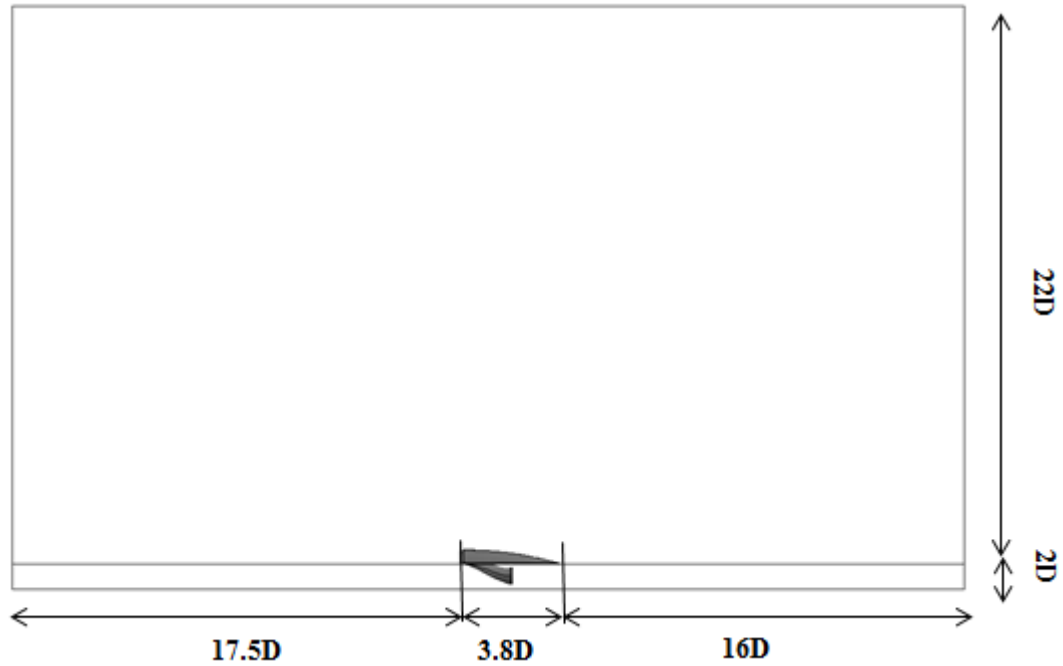


Figure 3-6 Solution Domain

Faces of the rectangular prism domain except for bottom face are defined as '*pressure far field*' boundary condition. The free-stream properties such as Mach number, pressure, temperature and flow direction are set for '*pressure far field*'. The inlet mounted face is defined as '*wall*'. In addition, engine face plane is set as '*pressure outlet*'.

Properties of freestream flow are given in Table 3-1.

Table 3-1 Fluid Properties

Mach Number	0.834
Reynolds Number	1.39×10^7
Fluid Type	Air
$P_{\text{static},\infty}$	19738 Pa
$T_{\text{static},\infty}$	216.65K
ρ	0.31738 kg/m^3

Value of $\dot{m}_{\text{corrected}}$ on engine interface is calculated as 0.463 kg/s at the wind tunnel test [26]. Since boundary conditions at pressure outlet are not presented in the paper, CFD analyses are performed to find average static pressure at engine interface for three different mesh qualities and different turbulence models. Results of CFD analyses are represented in Figure 3-7 and Figure 3-8. Static pressures at pressure outlet are selected for corrected mass flow rate equals to 0.463 kg/s for each mesh quality and turbulence model for the following analyses.

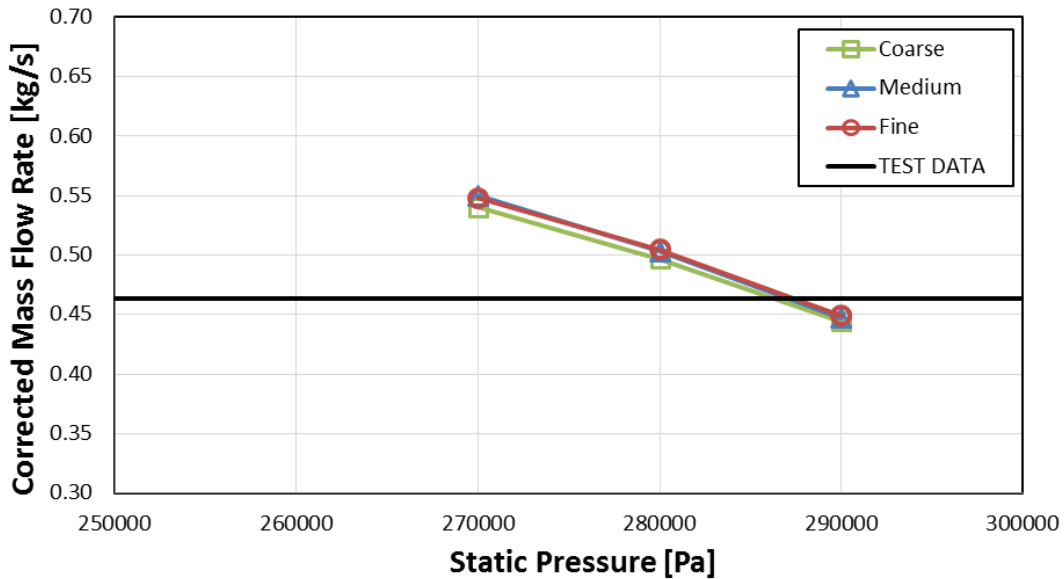


Figure 3-7 Corrected Mass Flow Rate Change for Different Mesh Qualities

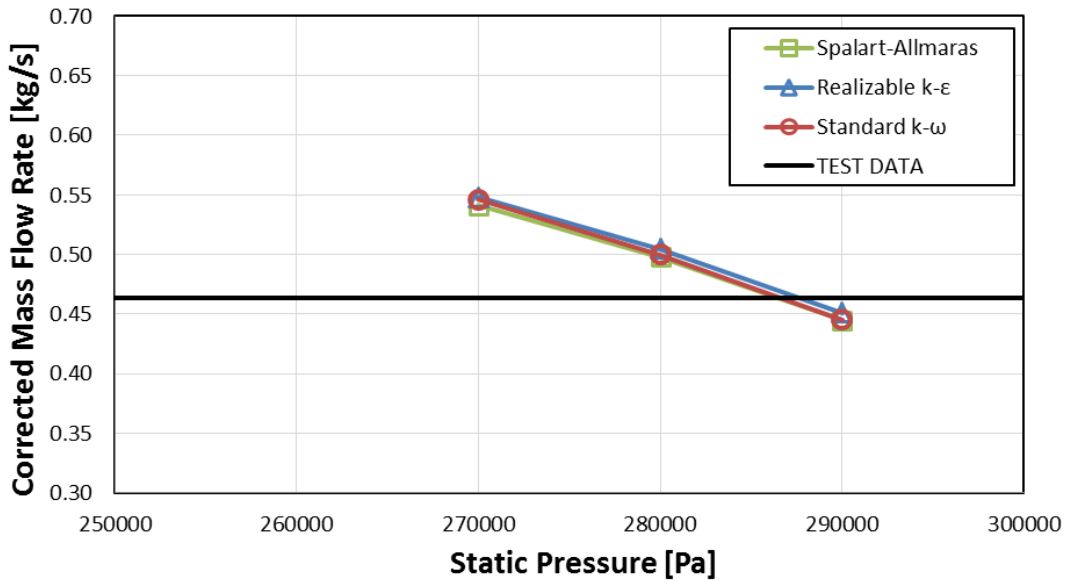


Figure 3-8 Corrected Mass Flow Rate Change for Different Turbulence Models

3.2.2 Mesh Independence Study

A grid sensitivity study is carried out in order to be sure about independency of the grid used in analyses. Three computational grids are generated to decide optimum acceptable grid size. Triangular unstructured surface mesh and volume mesh are generated by the GAMBIT software. Boundary layer grid is created by TGRID software.

Three different grids are examined which are coarse (855,618 cells), medium (2,733,878 cells) and fine (7,811,749 cells) meshes. The meshes are represented in Figure 3-9. In order to satisfy the enhanced wall treatment assumption, the equation $y^+ \approx 1$ must be satisfied. First 10 layers grow with 1.2 geometric grow rate and it has $1.5e^{-8} D_{inlet}$ first height. Remaining 25 layers grow by a condition which is the elements of last layer must have a height to length ratio of 50%.

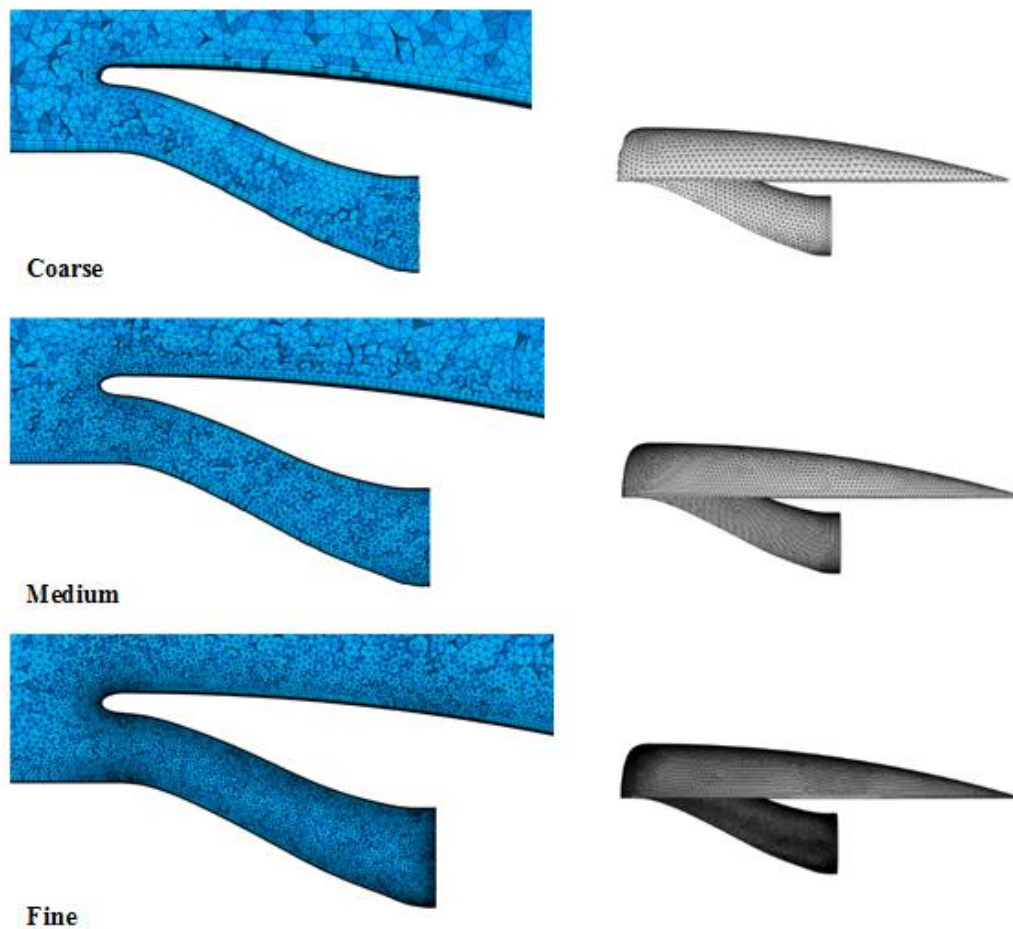


Figure 3-9 Coarse, Medium and Fine Mesh

For mesh convergence analyses, Realizable k-e turbulence model is used. Turbulence model study is carried out in the following section. The analyses are performed by using density based, steady, implicit solver.

Effect of mesh quality on the results is represented in Figure 3-10 and Figure 3-11. Mesh quality analyses show that mesh quality has a negligible effect on pressure recovery (PR) value. On the other hand, distortion coefficient (DC60) is sensitive to mesh quality. Fine and medium meshes give similar results for the DC60 value; however, coarse mesh gives unsatisfactory results. In order to save both time and computational power, medium mesh is chosen for the rest of the thesis study. Analyses are carried out for the case in which corrected mass flow rate at engine interface plane is 0.46 kg/s

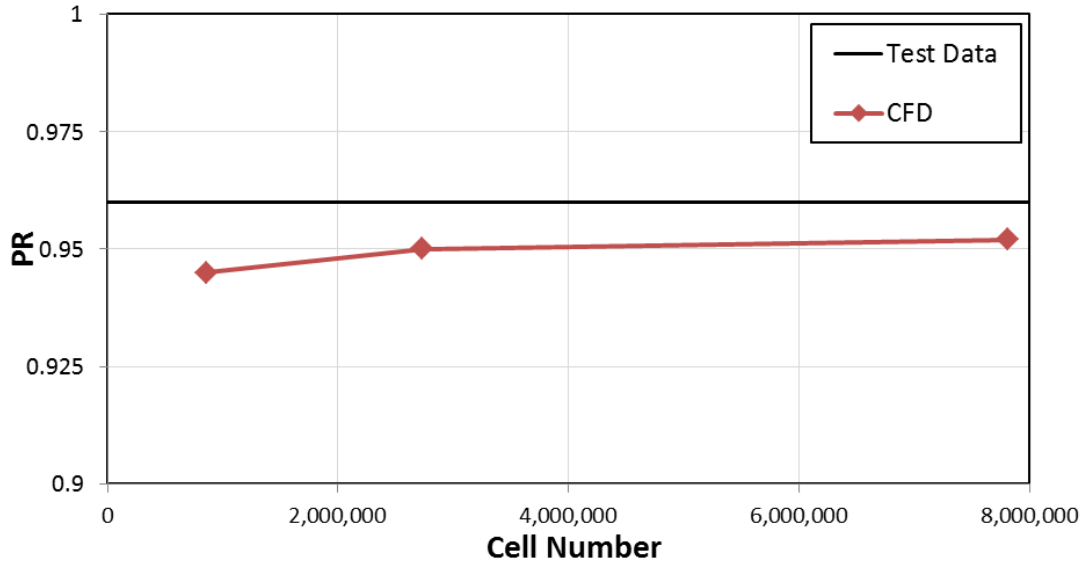


Figure 3-10 Pressure Recovery at AIP for Three Different Mesh Qualities
 ($\dot{m}_{corrected}=0.46$ kg/s)

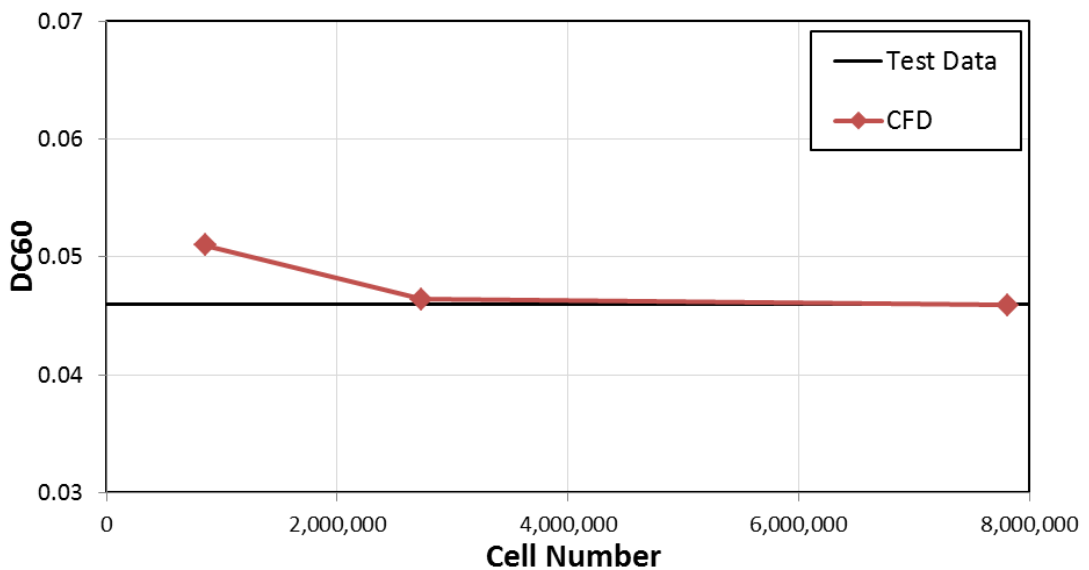


Figure 3-11 Distortion Coefficient at AIP for Three Different Mesh Qualities
 ($\dot{m}_{corrected}=0.46$ kg/s)

3.2.3 Turbulence Model Selection Study

Three different turbulence models Spalart-Allmaras, Realizable k- ϵ and Standard k- ω models results are compared with the test data in order to show the effect of

turbulence model on the PR and DC60. The results are represented in Figure 3-12 and Figure 3-13.

In Figure 3-12, turbulence models give very similar results and they under-predict PR value. While Realizable $k-\epsilon$ turbulence model predicts DC60 value well, Standard $k-\omega$ turbulence model over-predicts it. On the other hand, Spalart-Allmaras turbulence model under-predicts it. It can be said that Realizable $k-\epsilon$ and Standard $k-\omega$ give satisfactory results. On the other hand, Spalart-Allmaras give poor results comparing to other turbulence models.

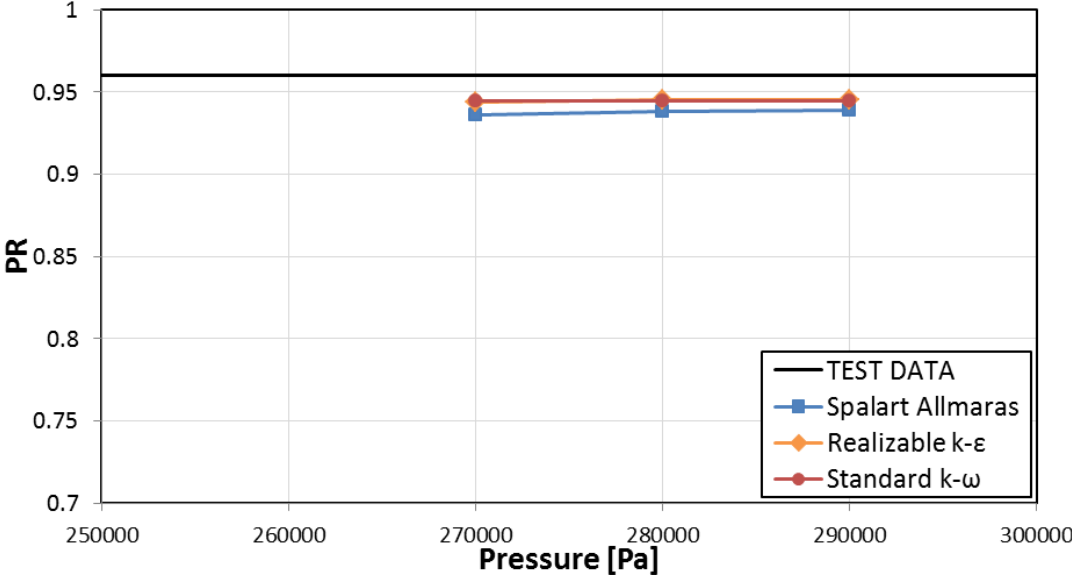


Figure 3-12 Pressure Recovery at AIP for Three Different Turbulence Models

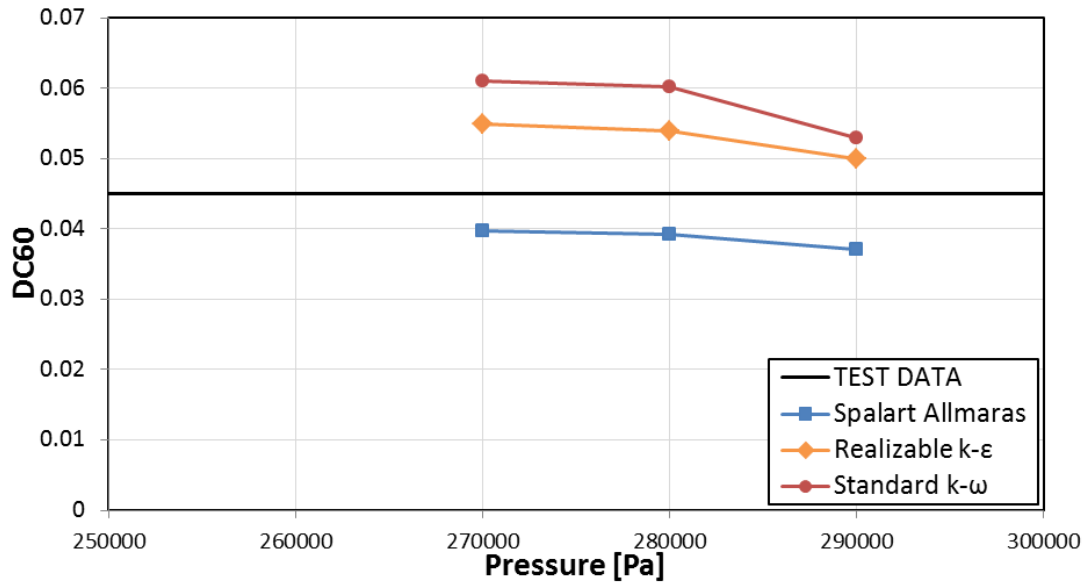


Figure 3-13 Distortion Coefficient at AIP for Three Different Turbulence Models

If calculated PR and DC60 values are compared with the experimental results, it can be concluded that current study gives satisfactory results. Fine mesh with Realizable k- ϵ turbulence model gives the best result; however there are negligible differences between fine mesh and medium mesh analyses results. In order to save time, medium mesh with k- ϵ turbulence model is used for the rest of the analyses.

3.2.4 Solution Domain Flow Visualization

Total pressure ratio contour at engine interface plane for different turbulence models are represented in Figure 3-14. As previously mentioned, low pressure regions are obtained because of secondary flow effects which are induced by S-duct inlet. Since low pressure regions in the CFD results are larger comparing to experimental data, it can be concluded that CFD performances are more pessimistic. This also explains the reason of lower PR value calculated at CFD analyses. The most similar total pressure distribution at engine interface plane to the test results is the one which is performed by using Realizable k- ϵ turbulence model.

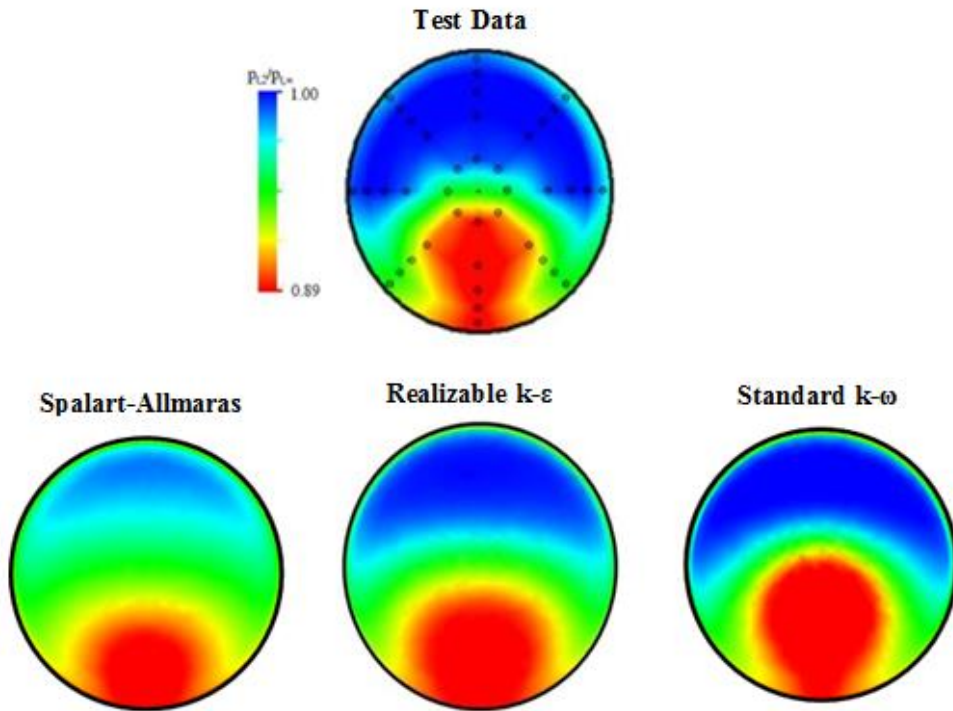


Figure 3-14 Total Pressure Contours at AIP for Three Different Turbulence Models

CHAPTER 4

RESULTS

In this part, analyses for different vortex generators designs are performed in order to improve the performance of inlet. Parameters of the vortex generators such as thickness, length, height, angle, number and location of vortex generators are changed and each of them is examined individually. Inlet is integrated to the missile body. Thus, the model used in the analyses is a long range missile with an inlet. The missile design Mach number is 0.85, so design of vortex generators are carried out for Mach number 0.85. A simplified model is represented in Figure 4-1.



Figure 4-1 Model

4.1 Solid Model and Mesh Generation

Since the body is the dominant part of the missile over the flow which goes into the inlet, protuberances on the missile surface such as wings, umbilical and fairing are not modeled in order to save time and computational power.

Fluid domain is large enough therefore boundary conditions at *'pressure far field'* is not affected by the flow over the missile. The fluid domain is cylinder with radius of 15 times length of the missile ($15L_{\text{missile}}$) and height of $45L_{\text{missile}}$. All faces of cylinder are set as *'pressure far field'*, surfaces of the missile and inlet are *'wall'* and engine face is selected as *'pressure outlet'*. Fluid domain and boundary conditions are given in Figure 4-2 and Figure 4-3.

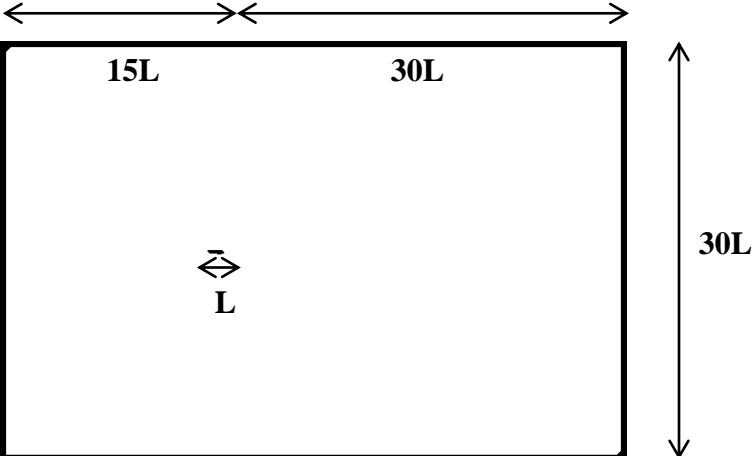


Figure 4-2 Dimensions of Fluid Domain

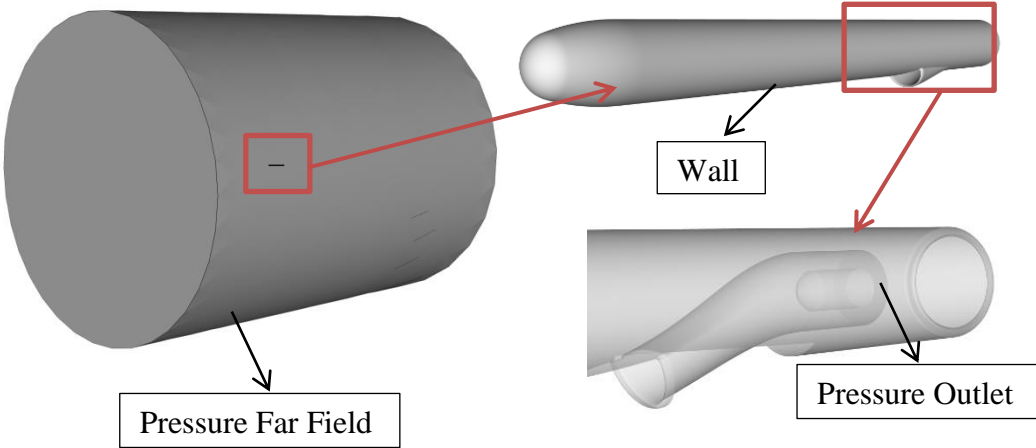


Figure 4-3 Boundary Conditions

There are 193,453 triangular surface elements and fluid domain contains 7,689,358 volume elements. Boundary layer is created by using TGRID by considering y^+ . Details of generated volume mesh are represented in Figure 4-4.

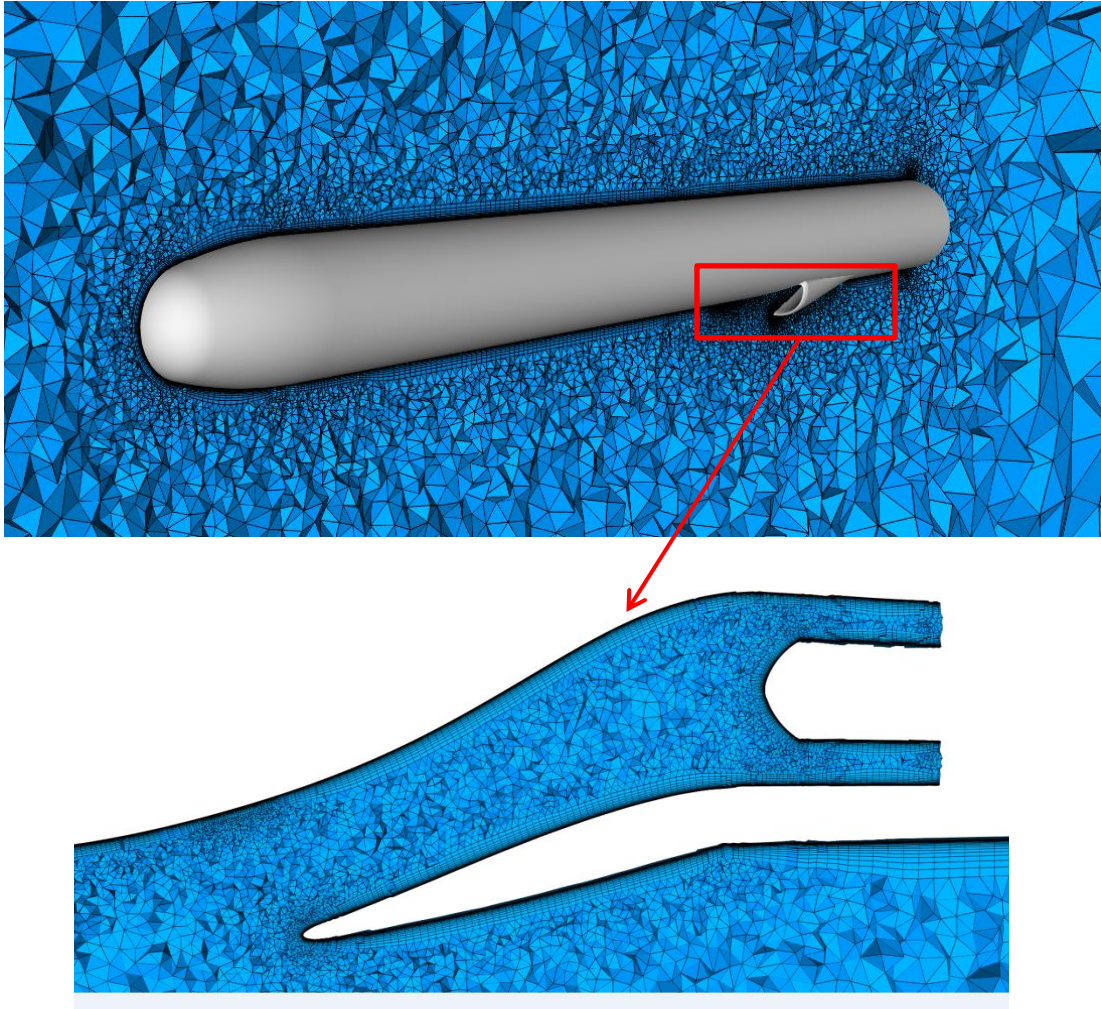


Figure 4-4 Detailed View of Volume Grid

4.2 Solution

In all CFD analyses, the Realizable k-e turbulence model is used since it gives better results for inlet analyses. Density based solver is chosen for analyses because of the missile design Mach number at high subsonic region. Implicit solver with Roe-FS flux splitting scheme is selected. Parallel computations are performed using 48 CPUs for each analysis. It took 12 hours to complete each analysis.

4.3 Results and Discussion

Solution procedure for inlet analyses is almost same as external flow analyses. The only difference is to set a static pressure for '*pressure outlet*' which satisfy desired

mass flow rate at AIP. The missile usually operates at low altitude with Mach number of 0.85 and an angle of attack of 2° during its flight. Therefore, vortex generator study is performed for this flight conditions. In addition, the results are also compared for angle of attacks of -10°, 0° and 10°.

Engine of the missile requires corrected mass flow rate of 5 kg/s. Since average static pressure is unknown at AIP, an iterative study is carried out to find average static pressure at AIP for given corrected mass flow rate. As it is represented in Figure 4-5, static pressure at AIP is found and set as 127.5 kPa for the boundary condition 'pressure outlet'.

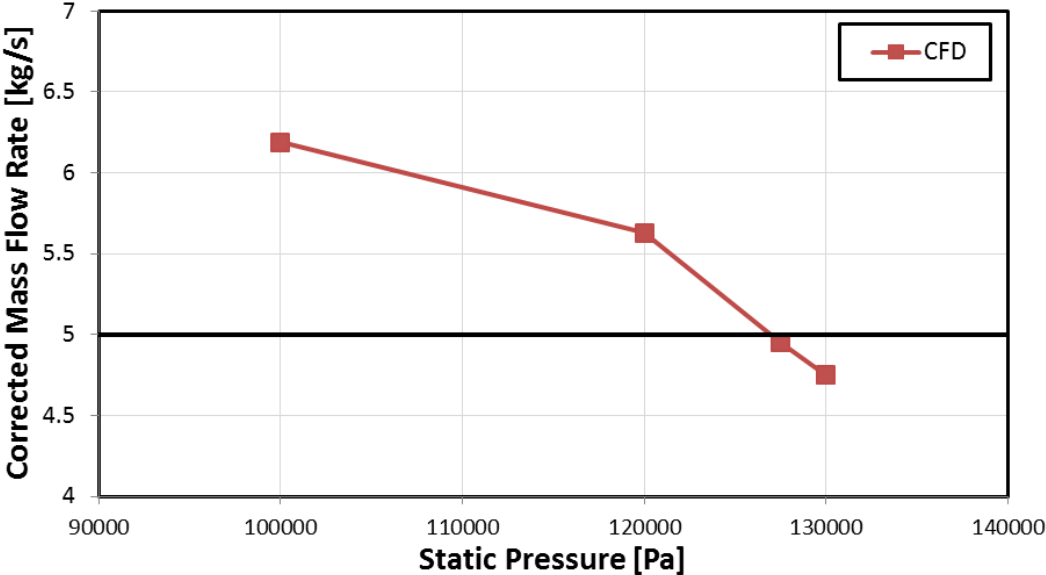


Figure 4-5 Corrected Mass Flow Rate Change for Different Static Pressures at AIP

Performance parameter of inlet PR is calculated as 0.944 which is satisfactory for the required engine performance. However, DC60 value 0.243 is not satisfactory since it is above the required DC60 value of 0.2. In the following parts of the thesis, several vortex generators are compared parametrically and their effects on DC60 are investigated.

4.3.1 Vortex Generators

Jet engines operate efficiently when they are supplied with uniform flow. In other words, low DC60 value which is less than 0.2 is desired at AIP. In order to reduce

DC60 value to acceptable levels and deliver more uniform flow to engine, parametric vortex generator design study is performed. In this study, vortex generators are placed at the entrance of inlet in order to make manufacturing process easier. Thus, location study of vortex generators is performed at a limited area. In addition, the vortex generators used in analyses are simple rectangular vane type and they are identical in shape. In this thesis, six different parameters which are orientation, height, length, thickness, position and number of vortex generators are examined and results are compared with the model INLET which is the base case without vortex generator. A sample of vortex generators is illustrated in Figure 4-6.

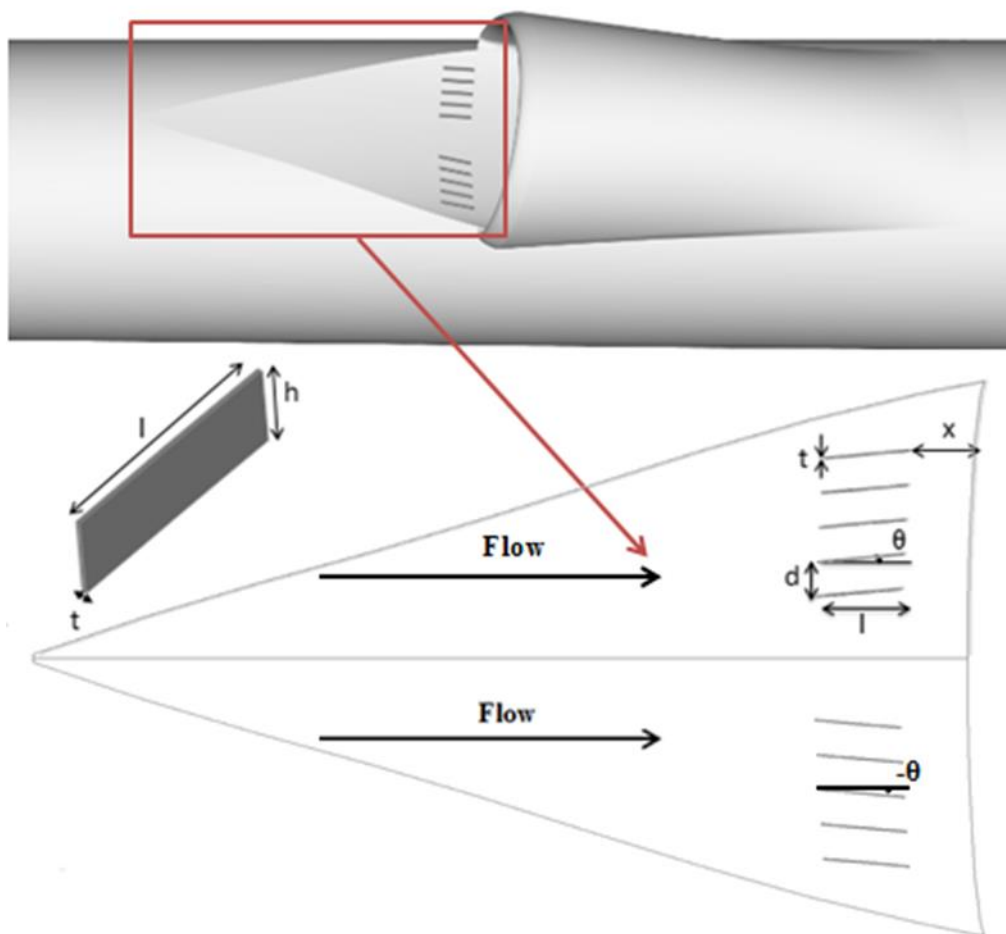


Figure 4-6 Vortex Generators on Missile Surface

4.3.1.1 Orientation of Vortex Generators

Orientation of vortex generators to the upcoming flow has a significant impact on the performance of an inlet. In order to obtain a symmetric geometry with respect to pitch plane, vortex generators are placed symmetrically with respect to pitch plane. Thus, half of them are located with positive angle to the upcoming flow while the remaining ones are placed with negative angle with same magnitude. Four different orientation angles are compared meanwhile other parameters are kept constant. Dimensions are given in the form of radius of AIP. INLET refers to the reference inlet which is the model without vortex generators. Configuration dimensions are given in Table 4-1.

Table 4-1 Vortex Generator Models with Different Orientations

Models.	$\theta(^{\circ})$	$h(R_{AIP})$	$l(R_{AIP})$	$t(R_{AIP})$	$x(R_{AIP})$	#of VGs
INLET	-	-	-	-	-	-
VG1	0	0.060	0.310	0.004	0.258	10
VG2	5	0.060	0.310	0.004	0.258	10
VG3	10	0.060	0.310	0.004	0.258	10
VG4	15	0.060	0.310	0.004	0.258	10

Four different models are designed and their performances are compared each other for four different angle of attack values which are -10° , 0° , 2° and 10° . VG1 is parallel to the upcoming flow and VG4 is oriented with highest angle to the upstream. For the cruise angle of attack 2° , DC60 values at AIP of these configurations are given in Figure 4-7. Dashed line represents the DC60 value of INLET.

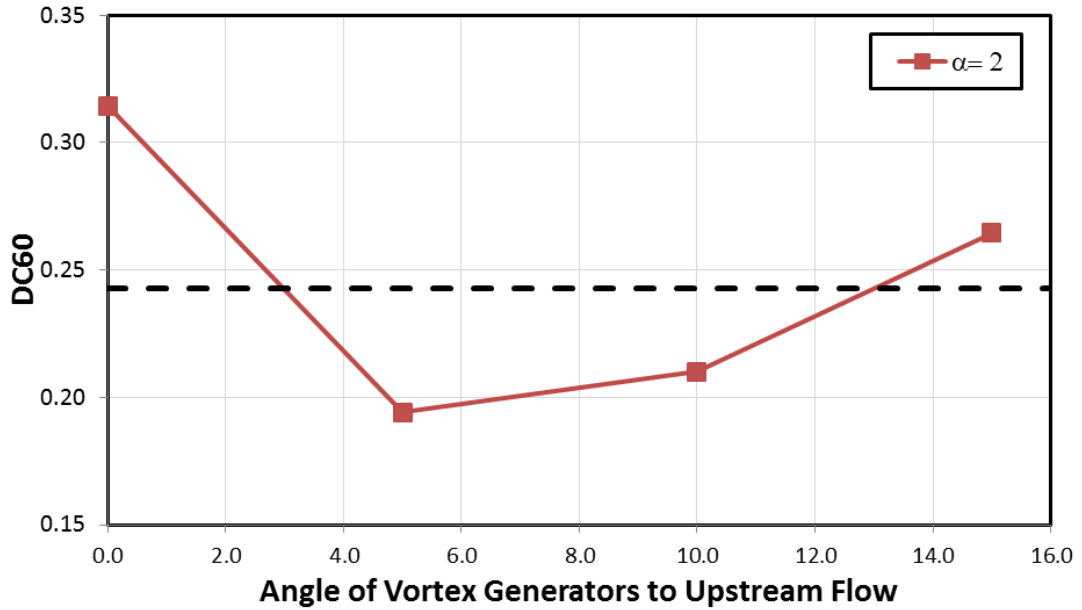


Figure 4-7 DC60 Values of Differently Oriented Vortex Generator Configurations

As it is seen from Figure 4-7, orientation to the upstream flow with an angle of 3°-13° improves the flow for cruise flight. The best improvement is obtained at the angle around 5°. PR and DC60 values for the configurations at cruise condition are tabulated in Table 4-2.

Table 4-2 Results of Vortex Generator Model with Different Orientations

Model	$\theta(^{\circ})$	$h(R_{AIP})$	$l(R_{AIP})$	$t(R_{AIP})$	$x(R_{AIP})$	#of VGs	DC60	Difference	PR
INLET	-	-	-	-	-	-	0.243	-	0.944
VG1	0	0.060	0.310	0.004	0.258	10	0.314	-29.4%	0.940
VG2	5	0.060	0.310	0.004	0.258	10	0.194	20.1%	0.942
VG3	10	0.060	0.310	0.004	0.258	10	0.21	13.5%	0.943
VG4	15	0.060	0.310	0.004	0.258	10	0.265	-8.9%	0.942

PR values for the vortex generator configurations decrease by insignificant amount. On the other hand, there is noteworthy improvement on flow uniformity of VG2 and VG3. For different angles of attack, differences in percentage of DC60 for the vortex generator models with respect to INLET model are represented in Figure 4-8.

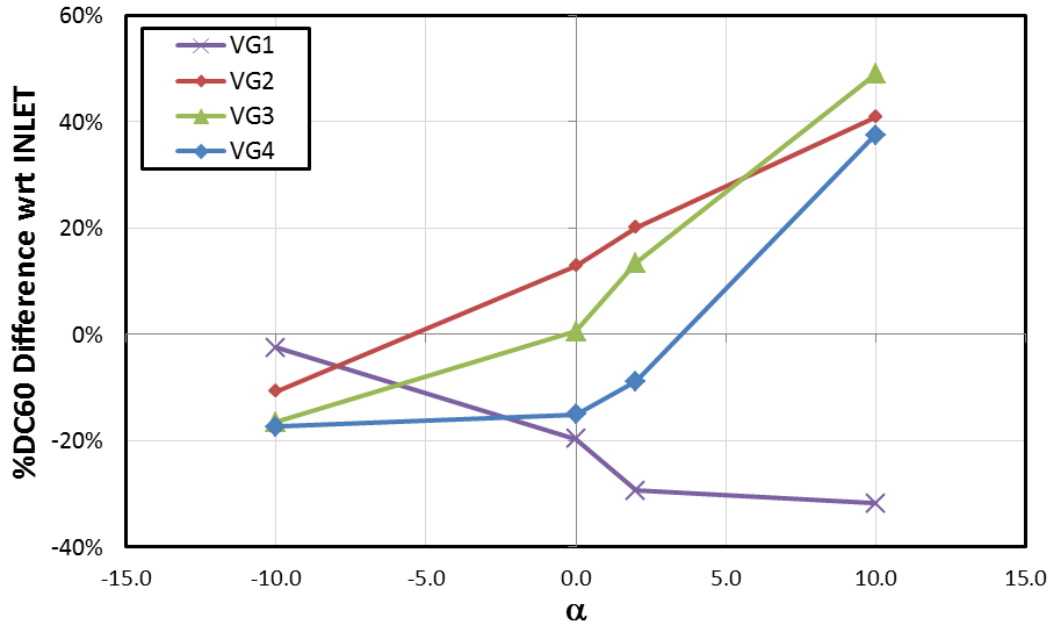


Figure 4-8 DC60 Difference with respect to INLET

The best improvement is obtained at the highest angle of attack 10° which is about 50% with respect to INLET. No improvement is observed for the design VG1. To conclude, for cruise flight conditions, placing vortex generator vanes with an angle between 3° to 13° to the upstream flow improves the flow. However, the flow non-uniformity increases for the angles above 13° with respect to the INLET. Since VG2 give best result for this parameter, VG2 model is kept as common configurations for all parameter studies.

4.3.1.2 Height of Vortex Generators

Height of vortex generators has also a significant impact on the performance of inlet. Since it is directly related to boundary layer thickness at the region where vortex generators are located, height of the vortex generators must be selected carefully. Four different heights are compared and other parameters are kept constant. Configuration dimensions are given in Table 4-3.

Table 4-3 Vortex Generator Models with Different Heights

Models	$\theta(^{\circ})$	$h(R_{AIP})$	$l(R_{AIP})$	$t(R_{AIP})$	$x(R_{AIP})$	#of VGs
INLET	-	-	-	-	-	-
VG5	5	0.043	0.310	0.004	0.258	10
VG2	5	0.060	0.310	0.004	0.258	10
VG6	5	0.086	0.310	0.004	0.258	10
VG7	5	0.129	0.310	0.004	0.258	10

Boundary layer thickness at the region where vortex generators are placed is about 0.07 times radius of AIP. VG5 and VG2 are submerged in boundary layer, while heights of VG6 and VG7 are higher than boundary layer thickness. For the cruise angle of attack 2° , DC60 values at AIP of these configurations are given in Figure 4-9. Dashed line represents the DC60 value of INLET.

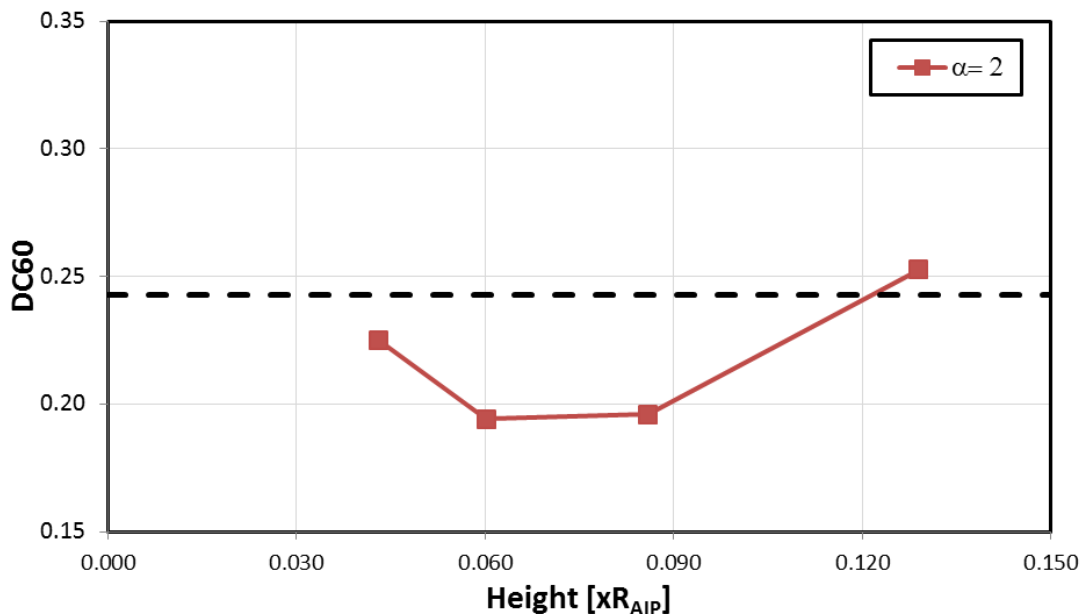


Figure 4-9 DC60 Values of Vortex Generator Configurations with Different Heights

Heights of vortex generators lower than 0.12 times radius of AIP improves the flow uniformity for cruise flight in Figure 4-9. If vortex generator vanes are too short, effectiveness of vortex generators reduces since they mix medium momentum flow with low momentum flow. Although vortex generator vanes with height higher than boundary layer thickness mix high momentum flow with low momentum flow, it spoils the freestream flow. Thus, the best improvement is obtained at the height 0.8-

1.2 times the boundary layer thickness which is 0.07 times radius of AIP. PR and DC60 values for the configurations are tabulated in Table 4-4.

Table 4-4 Results of Vortex Generator Model with Different Heights

Model	$\theta(^{\circ})$	$h(R_{AIP})$	$l(R_{AIP})$	$t(R_{AIP})$	$x(R_{AIP})$	#of VGs	DC60	Difference	PR
INLET	-	-	-	-	-	-	0.243	-	0.944
VG5	5	0.043	0.310	0.004	0.258	10	0.225	7.4%	0.942
VG2	5	0.060	0.310	0.004	0.258	10	0.194	20.1%	0.942
VG6	5	0.086	0.310	0.004	0.258	10	0.196	19.4%	0.942
VG7	5	0.129	0.310	0.004	0.258	10	0.253	-4.0%	0.941

As it is mentioned in previous section, PR values for these configurations also change by insignificant amount. However, there is improvement on DC60 value up to 20%. For different angles of attack, differences in percentage of DC60 for the vortex generator models with respect to INLET model are represented in Figure 4-10.

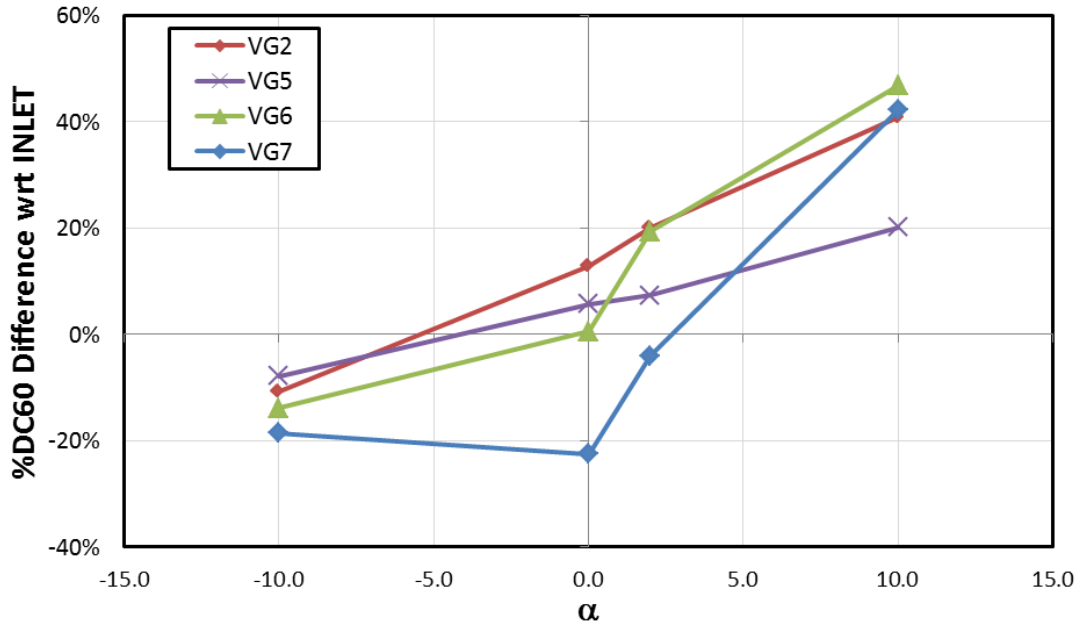


Figure 4-10 DC60 Difference with respect to INLET

Up to 45% improvement is obtained at the angle of attack 10° . The flow non-uniformity increased for the angle of attack -10° . Since the missile rarely operates at an angle of attack -10° , these data do not affect the overall performance of the inlet

with vortex generators. Placing vortex generator vanes with height of 0 to 0.12 times radius of AIP makes the flow more uniform. When the height of vortex generators are close to height of boundary layer at the studied area, the best improvement on the flow uniformity at AIP is obtained. In addition, the flow non-uniformity increases for the heights above 0.12 times radius of AIP. To sum up, before deciding height of vortex generators, boundary layer must be examined since it is directly related to performance of vortex generators.

4.3.1.3 Length of Vortex Generators

Since vortex generators direct the flow to different path, how long they accompany the flow is so important. Increasing length of vortex generations improves the performance of inlet however it is up to some point. In this section, five different lengths of vortex generators are compared. Dimensions belongs to different configurations are given in Table 4-5.

Table 4-5 Vortex Generator Models with Different Lengths

Models	$\theta(^{\circ})$	$h(R_{AIP})$	$l(R_{AIP})$	$t(R_{AIP})$	$x(R_{AIP})$	#of VGs
INLET	-	-	-	-	-	-
VG8	5	0.060	0.077	0.004	0.258	10
VG9	5	0.060	0.155	0.004	0.258	10
VG2	5	0.060	0.310	0.004	0.258	10
VG10	5	0.060	0.413	0.004	0.258	10
VG11	5	0.060	0.620	0.004	0.258	10

Five different models are designed and their performances are compared each other for five different lengths. For the cruise angle of attack 2° , DC60 values at AIP of these configurations are given in Figure 4-11. Dashed line represents the DC60 value of INLET.

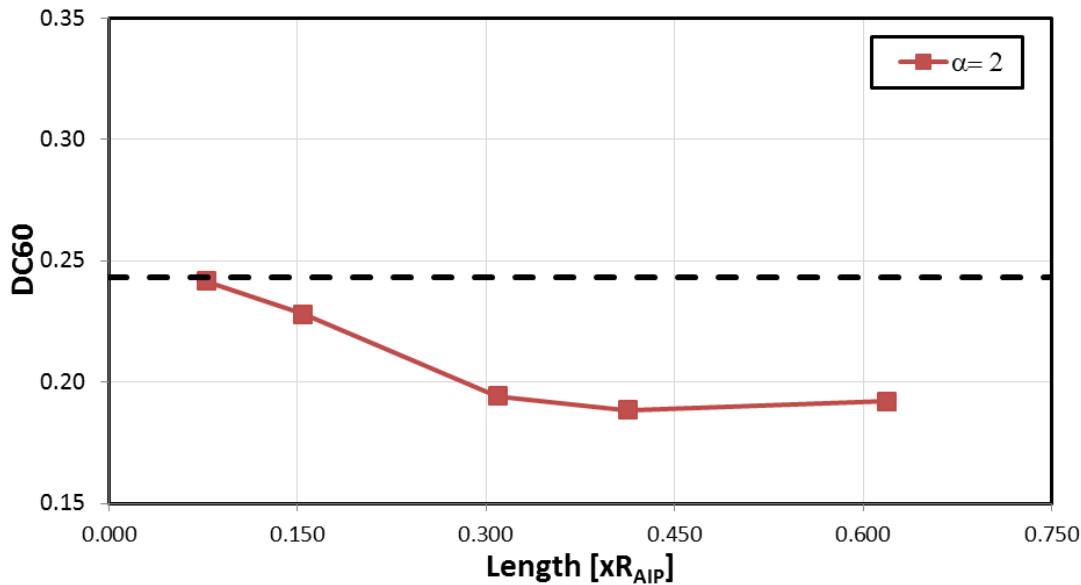


Figure 4-11 DC60 Values of Vortex Generator Configurations with Different Lengths

it is clearly seen from Figure 4-11, lengths of vortex generators higher than 0.075 times radius of AIP improves the flow uniformity for cruise flight. Vortex generators with lengths above 0.3 times radius of AIP improve the flow at almost same level for cruise condition. For angle of attack 2° , PR and DC60 values for the configurations are represented in Table 4-6.

Table 4-6 Results of Vortex Generator Model with Different Lengths

Model	$\theta(^{\circ})$	$h(R_{AIP})$	$l(R_{AIP})$	$t(R_{AIP})$	$x(R_{AIP})$	#of VGs	DC60	Difference	PR
INLET	-	-	-	-	-	-	0.243	-	0.944
VG8	5	0.060	0.077	0.004	0.258	10	0.242	0.6%	0.943
VG9	5	0.060	0.155	0.004	0.258	10	0.228	6.2%	0.943
VG2	5	0.060	0.310	0.004	0.258	10	0.194	20.1%	0.942
VG10	5	0.060	0.413	0.004	0.258	10	0.189	22.4%	0.942
VG11	5	0.060	0.620	0.004	0.258	10	0.192	21.0%	0.942

There is improvement on DC60 value up to 22.5% and maximum reduction on PR value is about 0.5% which is negligible. For different angles of attack, differences in percentage of DC60 for the vortex generator models with respect to INLET model are represented in Figure 4-12.

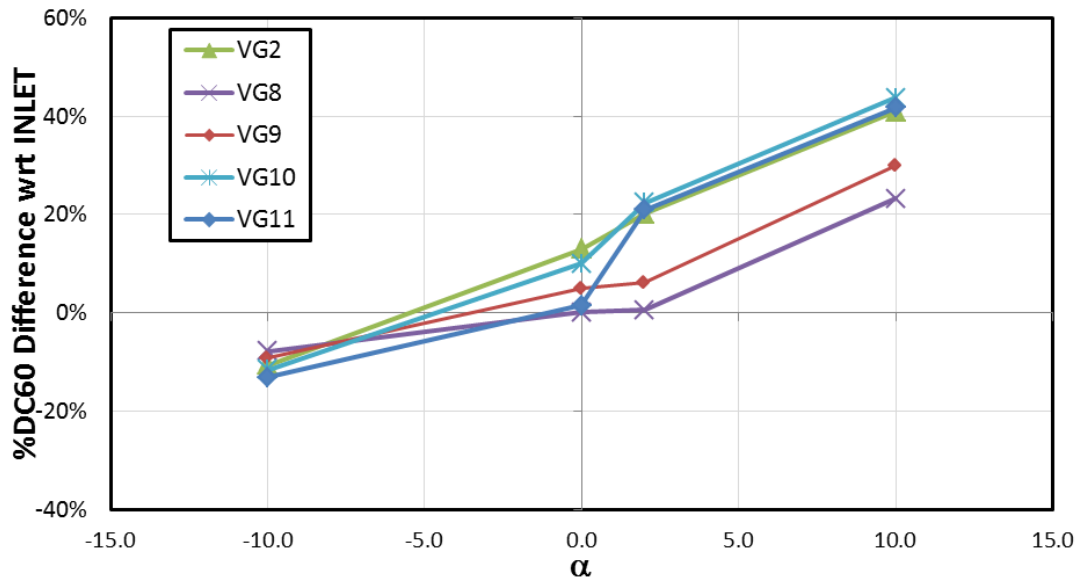


Figure 4-12 DC60 Difference with respect to INLET

At the highest angle of attack 10° , DC60 value decreases up to 42%. To summarize, placing vortex generator vanes with length above 0.075 times radius of AIP makes the flow more uniform. When the lengths of vortex generators are higher than 0.3 times radius of AIP up to 0.62 times radius of AIP, the improvement on the flow uniformity at AIP does not change with increasing length of vortex generators.

4.3.1.4 Thickness of Vortex Generators

Thick vortex generators have adverse effect on the inlet performance. Although thinner vortex generators are desired by designers, manufacturing limits must be also taken into account. Thinner vortex generators which have thickness below 0.004 times radius of AIP gives rise to a dramatic increase in manufacturing costs. Therefore, the vortex generator thicknesses used in the analyses is limited by 0.004 times radius of AIP. Three different thicknesses are compared and other parameters are kept constant. Dimensions of different configurations are given in Table 4-7.

Table 4-7 Vortex Generator Models with Different Thicknesses

Models	$\theta(^{\circ})$	$h(R_{AIP})$	$l(R_{AIP})$	$t(R_{AIP})$	$x(R_{AIP})$	#of VGs
INLET	-	-	-	-	-	-
VG2	5	0.060	0.310	0.004	0.258	10
VG12	5	0.060	0.310	0.009	0.258	10
VG13	5	0.060	0.310	0.013	0.258	10

Three different models are designed and their performances are compared each other for three different thicknesses. Although thinner vortex generators are desired, two thicker ones are analyzed in order to reduce manufacturing cost and integrating difficulties. For the cruise angle of attack 2° , DC60 values at AIP of these configurations are given in Figure 4-13.

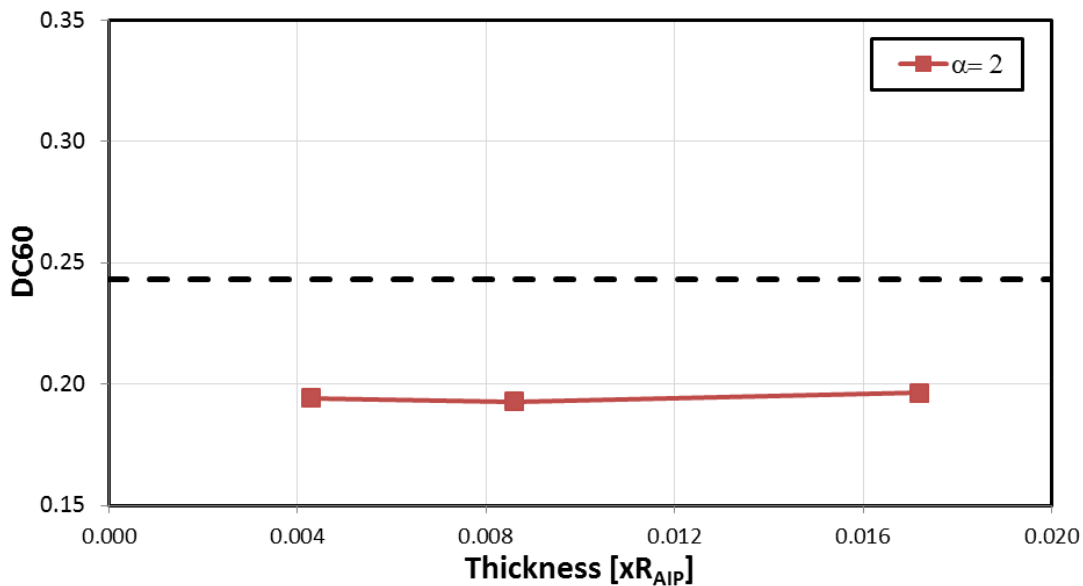


Figure 4-13 DC60 Values of Vortex Generator Configurations with Different Thicknesses

As it is seen from Figure 4-13, all vortex generator configurations improve the flow uniformity for cruise flight. Even though thickness of vortex generators has almost no effect on the performance of the inlet for cruise conditions, analyses for other flight conditions should also be investigated. Performances of configurations are more accurately compared in Figure 4-14. PR and DC60 values for the configurations at cruise condition are tabulated in Table 4-8.

Table 4-8 Results of Vortex Generator Model with Different Lengths

Model	$\theta(^{\circ})$	$h(R_{AIP})$	$l(R_{AIP})$	$t(R_{AIP})$	$x(R_{AIP})$	#of VGs	DC60	Difference	PR
INLET	-	-	-	-	-	-	0.243	-	0.944
VG2	5	0.060	0.310	0.004	0.258	10	0.194	20.1%	0.942
VG12	5	0.060	0.310	0.009	0.258	10	0.193	20.6%	0.941
VG13	5	0.060	0.310	0.013	0.258	10	0.196	19.2%	0.940

Although PR values for the configurations change by insignificant amount, it is clearly seen that PR value decreases with increasing thickness. On the other hand, improvement on DC60 value up to 20 % is obtained. Despite of other parameters, DC60 value does not change with changing thickness up to 0.013 times radius of AIP for cruise conditions. For different angles of attack, differences in percentage of DC60 for the vortex generator models with respect to INLET model are represented in Figure 4-14.

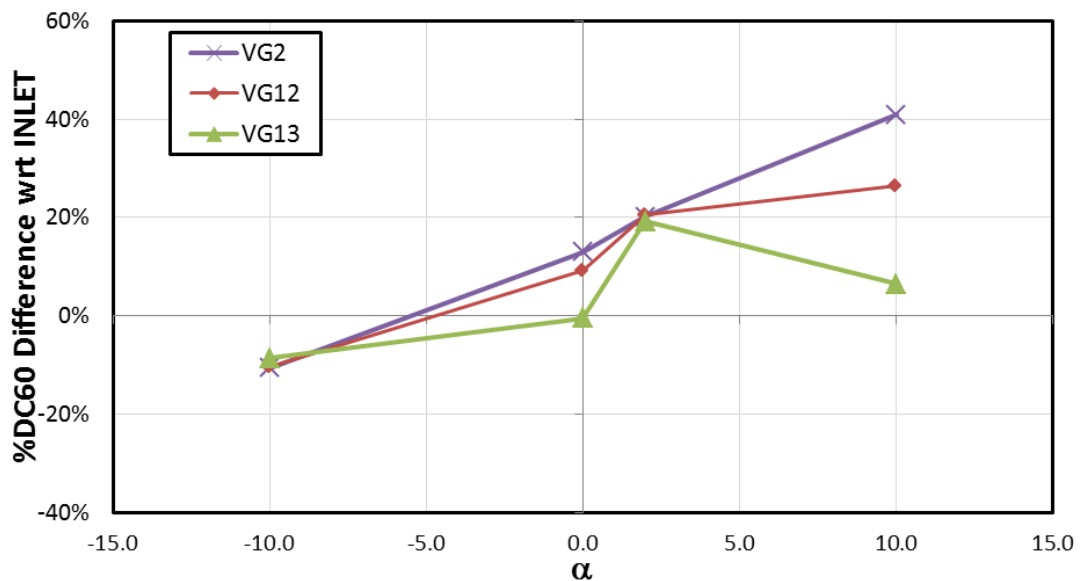


Figure 4-14 DC60 Difference with respect to INLET

The best improvement on DC60 is about 40% with respect to INLET. To conclude, for cruise condition, placing vortex generator vanes with thickness up to 0.013 times radius of AIP makes the flow more uniform. However, the improvement on the flow uniformity at AIP does not change with increasing thickness of vortex generators. Thinner vortex generators are desired when all flight conditions are considered;

however other configurations also give satisfactory performances for cruise conditions.

4.3.1.5 Position of Vortex Generators

Since vortex generators work better when they are placed before flow separation occurs, positions of vortex generations are very critical. By considering this phenomena and manufacturing possibilities, position of vortex generators are tested on a limited area in this study. Increasing x value means that distance between vortex generators and lip of inlet is increasing. In other words, vortex generators move through the upstream flow with increasing x parameter. Configuration dimensions are represented in Table 4-9.

Table 4-9 Vortex Generator Models at Different Positions

Models	$\theta(^{\circ})$	$h(R_{AIP})$	$l(R_{AIP})$	$t(R_{AIP})$	$x(R_{AIP})$	#of VGs
INLET	-	-	-	-	-	-
VG14	5	0.060	0.310	0.004	0.129	10
VG2	5	0.060	0.310	0.004	0.258	10
VG15	5	0.060	0.310	0.004	0.387	10
VG16	5	0.060	0.310	0.004	0.516	10

For cruise flight, DC60 values at AIP of these configurations are given in Figure 4-15.

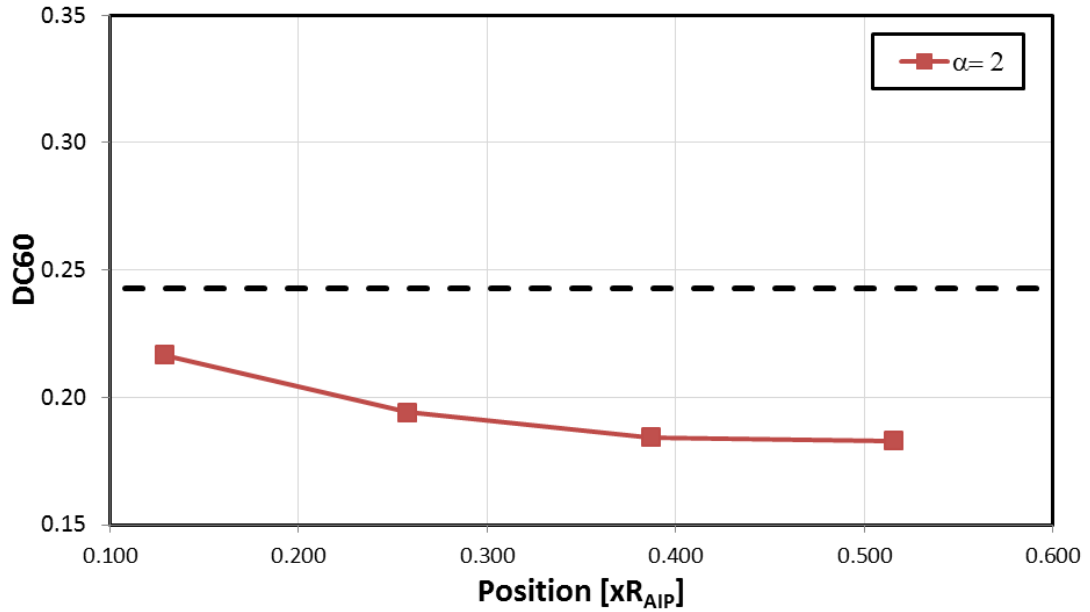


Figure 4-15 DC60 Values of Vortex Generator Configurations with Different Positions

Distance of vortex generators from inlet lip higher than 0.12 times radius of AIP improves the flow uniformity for cruise flight in Figure 4-15. Moreover, vortex generators with a distance 0.3-0.52 times radius of AIP to inlet lip improve the flow at almost same degree. PR and DC60 values for the configurations at cruise condition are tabulated in Table 4-10.

Table 4-10 Results of Vortex Generator Model with Different Lengths

Model	$\theta(^{\circ})$	$h(R_{AIP})$	$l(R_{AIP})$	$t(R_{AIP})$	$x(R_{AIP})$	#of VGs	DC60	Difference	PR
INLET	-	-	-	-	-	-	0.243	-	0.944
VG14	5	0.060	0.310	0.004	0.129	10	0.217	10.9%	0.943
VG2	5	0.060	0.310	0.004	0.258	10	0.194	20.1%	0.942
VG15	5	0.060	0.310	0.004	0.387	10	0.184	24.1%	0.943
VG16	5	0.060	0.310	0.004	0.516	10	0.183	24.7%	0.943

DC60 differences with respect to INLET with different angle of attack are represented in Figure 4-16.

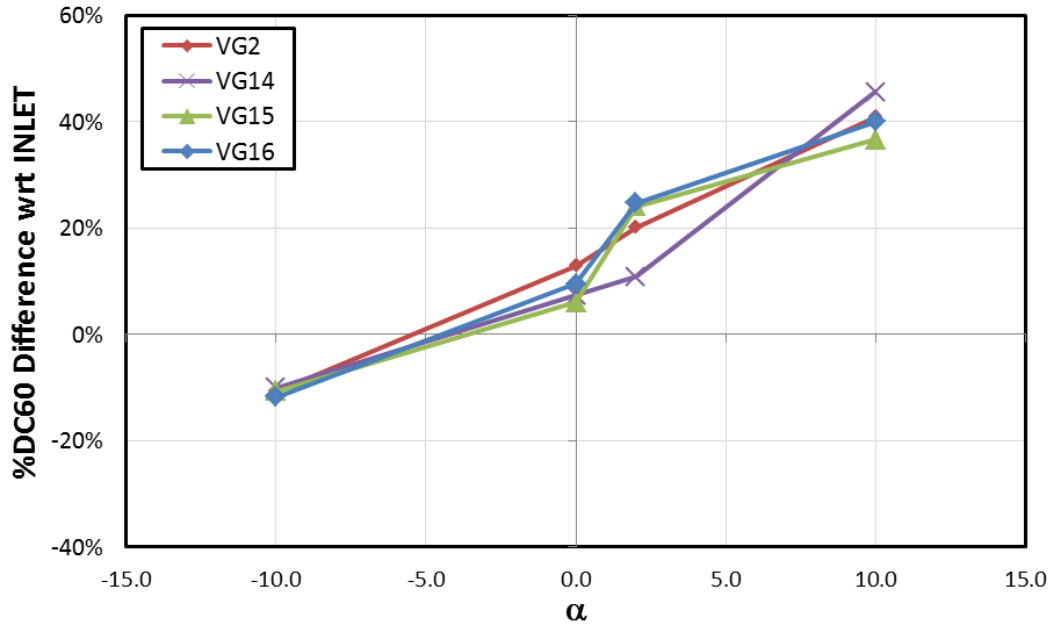


Figure 4-16 DC60 Difference with respect to INLET

DC60 value decreases by 50% with respect to INLET at angle of attack 10° for VG14. To sum up, placing vortex generator vanes with a distance of 0.12-0.52 times radius of AIP from inlet lip makes the flow more uniform. Vortex generators can be located at a highest distance of 0.52 times radius of AIP from inlet lip to obtain better performance.

4.3.1.6 Number of Vortex Generators

Number of vortex generations depends on inlet and vortex generators dimension. High number of vortex generators can increase drag, non-uniformity and PR reduction, while low number of vortex generators can affect the flow poorly. In this section, five different numbers of vortex generators are compared and other parameters are kept constant. Configuration dimensions are given in Table 4-11.

Table 4-11 Vortex Generator Models with Different Numbers

Models	$\theta(^{\circ})$	$h(R_{AIP})$	$l(R_{AIP})$	$t(R_{AIP})$	$x(R_{AIP})$	#of VGs
INLET	-	-	-	-	-	-
VG17	5	0.060	0.310	0.004	0.258	4
VG18	5	0.060	0.310	0.004	0.258	8
VG2	5	0.060	0.310	0.004	0.258	10
VG19	5	0.060	0.310	0.004	0.258	16
VG20	5	0.060	0.310	0.004	0.258	20

Five different models are designed and their performances are compared each other for five different numbers. For the cruise angle of attack 2° , DC60 values at AIP of these configurations are given in Figure 4-17.

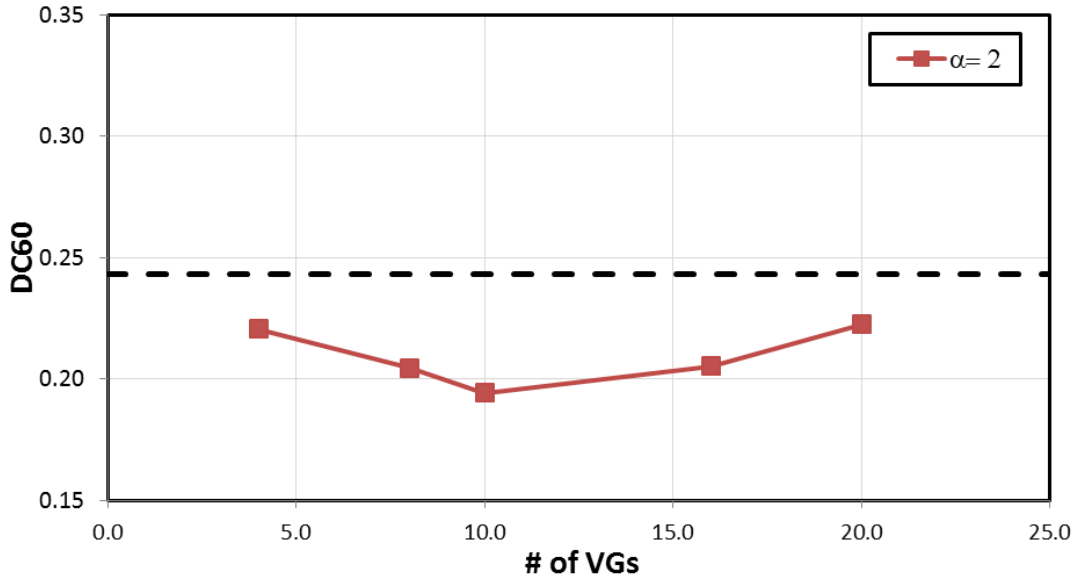


Figure 4-17 DC60 Values of Vortex Generator Configurations with Different Positions

Number of vortex generators lower than 20 improves the flow uniformity for cruise flight. Furthermore, the best improvement is obtained for the case which includes 10 vortex generator vanes. PR and DC60 values for the configurations are tabulated in Table 4-12.

Table 4-12 Results of Vortex Generator Model with Different Numbers

Model	$\theta(^{\circ})$	$h(R_{AIP})$	$l(R_{AIP})$	$t(R_{AIP})$	$x(R_{AIP})$	#of VGs	DC60	Difference	PR
INLET	-	-	-	-	-	-	0.243	-	0.944
VG17	5	0.060	0.310	0.004	0.258	4	0.220	9.3%	0.943
VG18	5	0.060	0.310	0.004	0.258	8	0.205	15.8%	0.943
VG2	5	0.060	0.310	0.004	0.258	10	0.194	20.1%	0.942
VG19	5	0.060	0.310	0.004	0.258	16	0.205	15.6%	0.941
VG20	5	0.060	0.310	0.004	0.258	20	0.222	8.5%	0.940

PR values for the configurations decrease with increasing number of vortex generators. On the other hand, Improvement on DC60 value up to 20 % is observed in results. DC60 differences with respect to INLET with different angle of attack are represented in Figure 4-18.

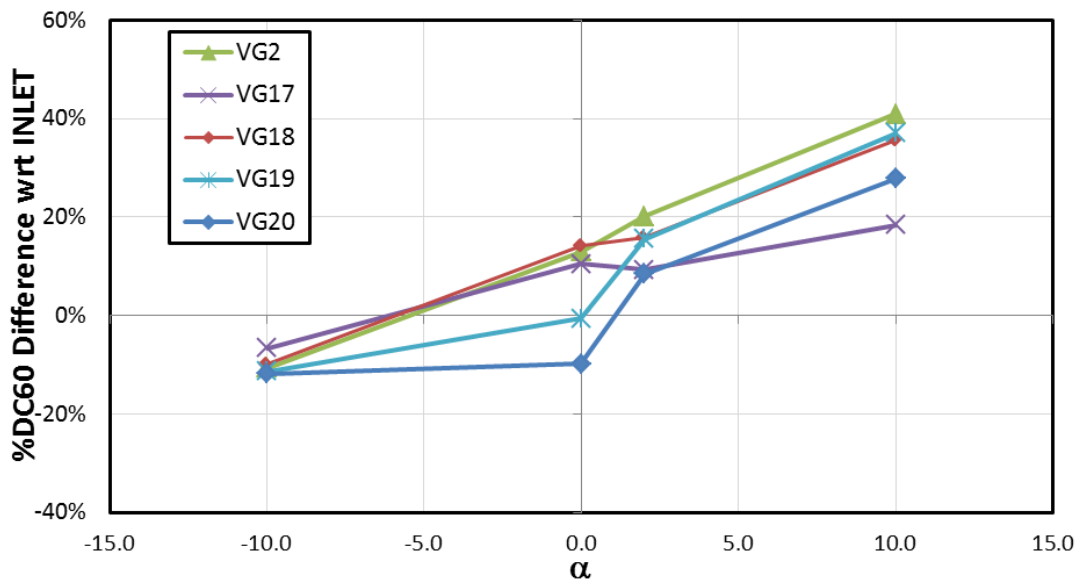


Figure 4-18 DC60 Difference with respect to INLET

DC60 decreases by 40% with respect to INLET at an angle of attack 10° for the configuration VG2. To summarize, optimum number or vortex generators can be found by a couple of iterative studies. For this case, the best performance is observed by placing 10 vortex generator vanes.

4.4 Post Process

In previous section, VG2 is used as the common configuration for all parameter studies. VG2 configuration results are satisfactory and its DC60 performance change with respect to INLET is linear. Therefore, comparison results between the configurations INLET and VG2 are represented by both data and visual in this section. DC60 difference with respect to INLET with different angles of attack is represented in Figure 4-19.

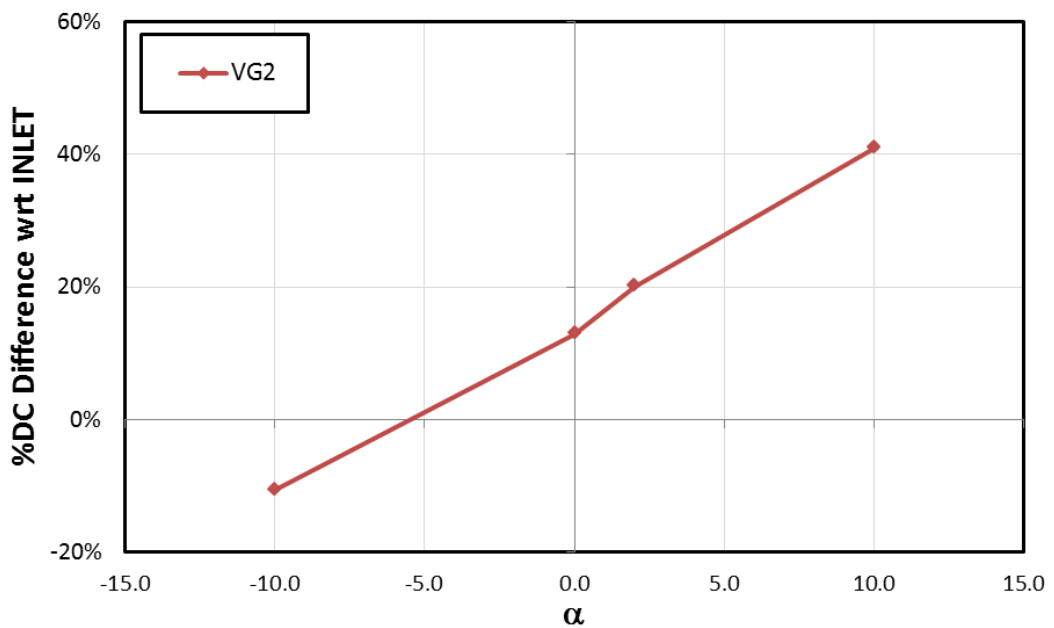


Figure 4-19 DC60 Difference between VG2 and INLET

As it is seen from Figure 4-19, improvement on DC60 value is obtained for the angle of attack above -5° . Since the maximum DC60 difference between INLET and VG2 is at the angle of attack of 10° , following data and figures are represented in this condition in order to see the improvement on flow uniformity more clearly.

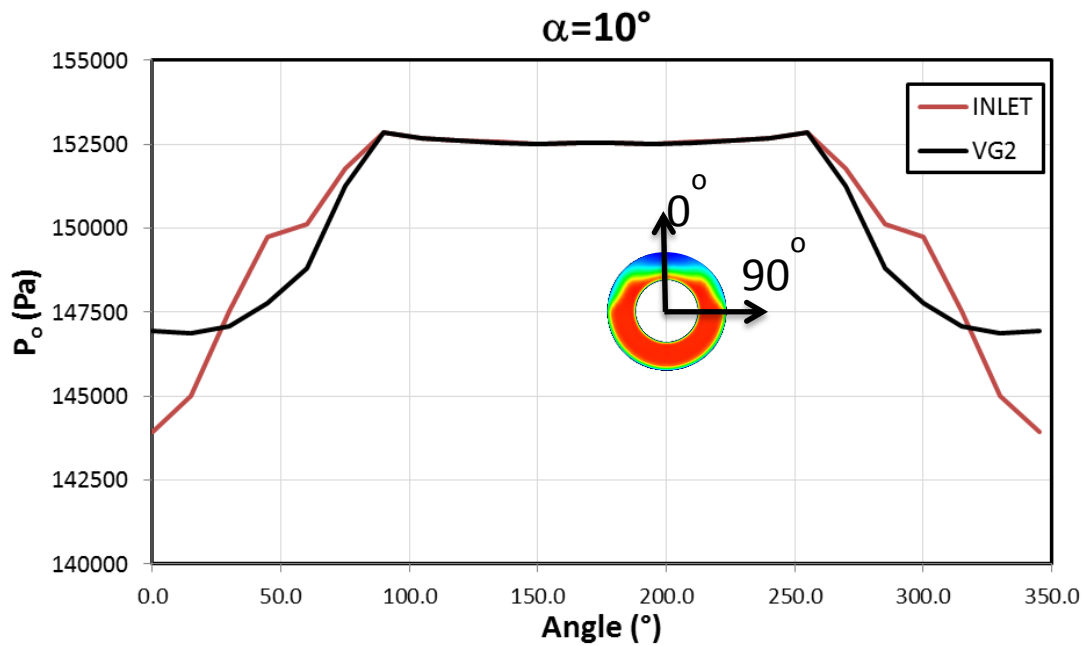


Figure 4-20 Average Total Pressure Distribution along Circumferential Direction at AIP

Average total pressure distribution along circumferential direction at AIP is represented in Figure 4-20. For a uniform flow at AIP, average total pressure distribution along circumferential direction is desired to be close each other. Vortex generators have no effects on the region which is between 90° to 270° . On the other hand, smallest average total pressure value increases from 142.5 kPa to 147 kPa at 0° . Although vortex generators decreases average total pressure between 25° and 90° , they obtain more uniform flow by improving the flow over low energy area. Total pressure contours of these two configurations are compared in Figure 4-21.

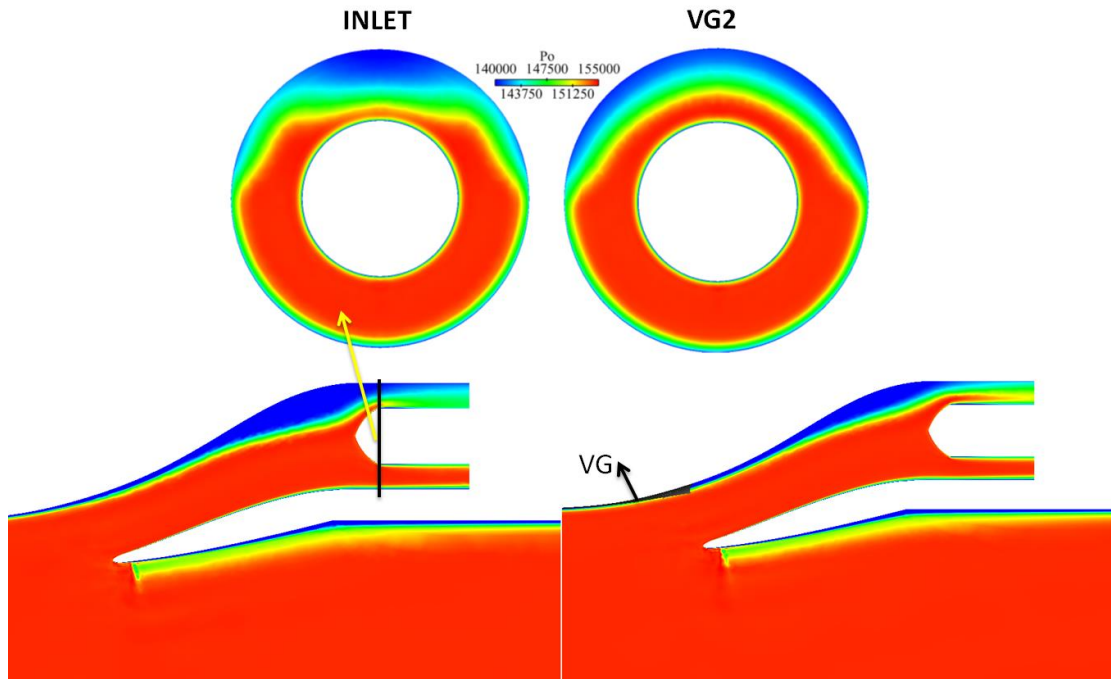


Figure 4-21 Total Pressure Contours of INLET and VG2 Configurations

Total pressure contours of the INLET and VG2 configurations at pitch plane and AIP are compared visually in Figure 4-21. The main problematic area is at top of the inlet where low momentum flow exists due to separation. By usage of vortex generators, there is considerable thinning at low energy region. It is because vortex generators increase energy of low momentum flow with high momentum flow. When contours of AIPs are examined, it can be concluded that even though average total pressure at AIP does not change, the flow becomes more uniform at AIP. Energy is fed to low momentum flow at top of the AIP by high momentum flow. Thus, low momentum flow region becomes smaller. Vectoral representations of the flow in the inlet with highlighted view of problematic area are represented in Figure 4-22 and Figure 4-23 for INLET and VG2 respectively.

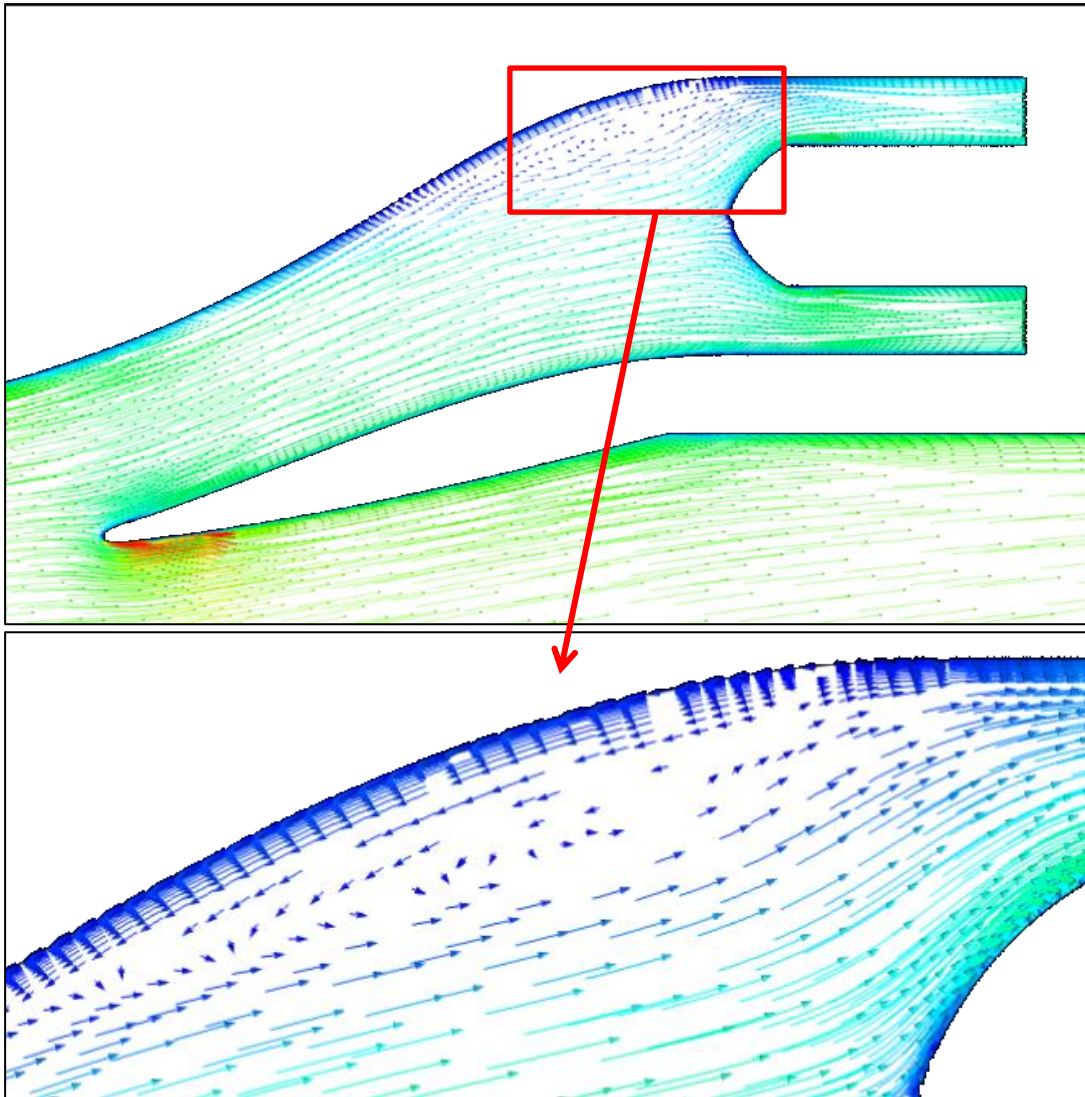


Figure 4-22 Vectorial Representation of the Flow in Inlet for Configuration INLET

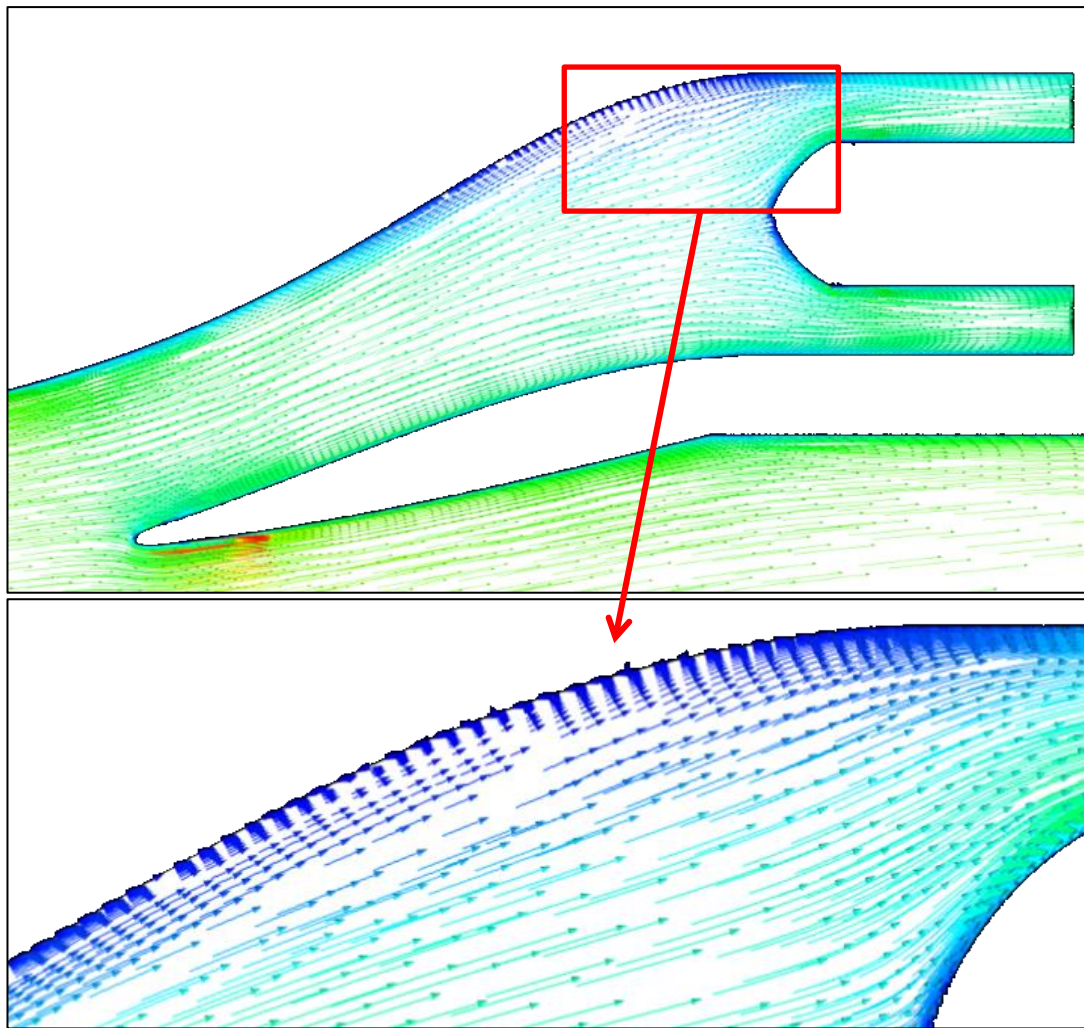


Figure 4-23 Vectoral Representation of the Flow in Inlet for Configuration VG2

In Figure 4-22, secondary flow in the low pressure region is observed. Flow is rotating and it is desired to eliminate secondary flows to deliver uniform flow to the engine. In Figure 4-23, vortex generators diminishes secondary flow and reverse flow to freestream flow is not observed anymore. Decreasing distortion in the flow inside the duct also reduces distortion at AIP. Despite of negligible PR reduction, vortex generators improve flow quality inside the duct and provide more uniform flow to the engine.

CHAPTER 5

CONCLUSION AND FUTURE WORK

5.1 Conclusion

Design of vortex generators for inlets has played an important role to control the flow separation and reduce inlet-engine interface distortion. Design process for vortex generators by experiments and tests are very expensive. Therefore, limited number of vortex generator designs can be tested in the design process. Meanwhile, by development of computer technology and CFD tools capabilities, inlet flows with vortex generators can be solved numerically. Thus, parametric design studies to the problem can be applied with available tools.

Inlet-A which is designed by the Boeing Company, is used as a test case in order to examine the applicability of this study. After grid independence and turbulent model selection studies are carried out, medium mesh quality and Realizable k- ϵ turbulence model are selected for the rest of the analyses. Results of validation analyses have satisfactory accuracy when they are compared with test results.

Parametric vortex generator design for the missile inlet is studied with validated CFD tools and methods. Each parameter examined individually and following statements are concluded. Vortex generators should be oriented with respect to freestream flow within a certain angle range. Height of vortex generators should be selected around boundary layer thickness. Increasing length of vortex generators improve the flow quality. Changes in thickness of vortex generators up to $0.013R_{AIP}$ have almost no effect on performance of vortex generators. Changing position of vortex generators at a limited region (a distance of 0.12-0.52 R_{AIP} to inlet lip) toward to upcoming flow increases vortex generator performance. Although four vortex generators improve flow, it is insufficient. On the other hand, twenty vortex generators increase non-

uniformity since it disturbs the uniform flow. Therefore, moderation in number of vortex generators provides better improvement on the flow quality.

Results show that usage of vortex generators can improve the quality flow uniformity of flow for most of the flight conditions. Even though insignificant amount (less than 1%) of reduction in PR value is obtained, 25% improvement of DC60 is achieved for cruise flight conditions. Considering whole flight range, improvement on DC60 value reaches up to 50%. It is concluded that, present study can be used in the vortex generator design for the high subsonic inlets. Moreover, vortex generator design depends on flight conditions and specific inlet geometry. Thus, this affect must be taken into account during vortex generator design processes.

5.2 Future Work

In the current study, only conventional types of vortex generators which are located outside of the inlet are modeled. Moreover, all studied vortex generator vanes are rectangular type with same orientations. Since there are some other usages of vortex generators located inside the duct in the literature, current study will be continued with vortex generators placed inside the inlet. In addition, vortex generators with different geometries such as triangular and airfoil type will be examined. Furthermore, only one set of vortex generators is used in current study. In future, a couple of set of vortex generators at different locations are examined. By this way, more uniform flow can be expected in expense of PR reduction.

REFERENCES

- [1] J. D. Anderson, "Introduction to Flight," 2004.
- [2] R. P. Akshoy, K. Kalyan, S. Y. Mahendra and D. Ujjal, "Flow Improvement in Rectangular Air Intake by Submerged Vortex Generators," Allahabad, India.
- [3] J. C. Dudek, "An Empirical Model for Vane-Type Vortex Generators in a Navier Stokes Code," NASA Technical Memorandum, Nevada, February 2005.
- [4] I. L. Peppler, "From The Ground Up," ISBN 0-9690054-9-0, 1996.
- [5] B. H. Anderson and R. Levy, "Vortex Generator Design for Aircraft Inlet Distortion as a Numerical Optimization Problem," Third International Conference on Inverse Design Concepts and Optimization in Engineering Sciences, Washington D.C., 1991.
- [6] L. Jaw, W. Cousins, D. N. Wu and D. Bryg, "Design and Test of a Semi-Passive Flow Control Device for Inlet Distortion Suppression," Journal of Turbomachinery, 2001.
- [7] J. Hamstra, D. Miller, P. Truax, B. Anderson and B. Wendt, "Active Inlet Flow Control Technology Demonstration," International Council of the Aeronautical Sciences, 2000.
- [8] B. Berrier and B. Allan, "Experimental and Computational Evaluation of Flush-Mounted, S-Duct Inlets (Invited)," NASA Langlet Research Center, Hampton, Virginia, 2004.
- [9] H. D. Taylor, "Application of Vortex Generator Mixing Principle of Diffusers," United Aircraft Corp. Research Dept, East Hartford, CT, 1948.
- [10] H. H. Percy and C. M. Stuart, "Methods of Boundary-Layer Control for Postponing and Alleviating Buffeting and other Effects of Shock-Induced Separation," IAS National Summer Meeting, Los Angeles, CA, 1959.
- [11] E. F. Valentine and R. B. Carrol, "Effects of Some Arrangements of Rectangular

- Vortex Generators on the Static Pressure Rise Through a Short 2:1 Diffuser," NASA, 1951.
- [12] G. Kaldschmidt, B. E. Syltedo and C. T. Ting, "727 Airplane Center Duct Inlet Low-Speed Performance Confirmation Model Test for Refanned JT8D Engines," NASA, 1973.
- [13] B. H. Anderson and R. Levy, "A Design Strategy for the Use of Vortex Generators to Manage Inlet-Engine Distortion Using Computational Fluid Dynamics," NASA, 1991.
- [14] B. J. Wendt and B. A. Reichert, "Vortex Ingestion in a Diffusing S-Duct Inlet," Journal of Aircraft, 1996.
- [15] B. A. Reichert and B. J. Wendt, "An Experimental Investigation of S-Duct Flow Control Using Arrays of Low-Profile Vortex Generators," AIAA 31st Aerospace Sciences Meeting and Exhibit, 1993.
- [16] A. J. Anabtawi, R. F. Blackwelder, P. B. S. Lissaman and R. H. Liebeck, "An experimental Investigation of Boundary Layer Ingestion in a Diffusing S-Duct with and without Passive Flow Control," AIAA Paper.
- [17] S. A. Gorton, L. R. Owens, L. N. Jenkins, B. G. Allan and E. P. Schuster, "Active Flow Control on a Boundary-Layer-Ingesting Inlet," AIAA Paper, 2004.
- [18] Buning P.G., Jespersen D. C., Pulliam T.H, W. M. Klopher, W. M. Chan, J. P. Slotnick, Krist S. E. and Renze K. J., "OVERFLOW User's Manual," NASA Langley Research Center, 1999.
- [19] G. A. Brian and R. O. Lewis, "Numerical Modeling of Flow Control in a Boundary-Layer-Ingesting Offset Inlet Diffuser at Transonic Mach Numbers," American Institute of Aeronautics and Astronautics.
- [20] G. Wheeler, "Means for Maintaining Attached Flow of a Flow Medium," U.S. Patent No 4455045, 1984.
- [21] K. A.M., "Boundary Layer Control of Flow Separation and Heat Exchange," U.S Patent No 3516264 (1971) and 3741285 (1973).
- [22] D. M. Rao and T. T. Kariya, "Boundary-Layer Submerged Vortex Generators for Separation Control- An Exploratory Study," Vigyan Research Associates, Inc., Hampton, Virginia.

- [23] J. Blazek, "Computational Fluid Dynamics: Principles and Applications," Elsevier, 2001.
- [24] "ANSYS FLUENT Theory Guide," 2009.
- [25] B. Berrier and M. Morehouse, "Evaluation of Flush-Mounted, S-Duct Inlets with Large Amounts of Boundary Layer Ingestion," NASA Langley Research Center, Hampton, Virginia.
- [26] B. L. Berrier, M. B. Carter and B. G. Allan, "High Reynolds Number Investigation of a Flush-Mounted, S-Duct Inlet with Large Amounts of Boundary Layer Ingestion," Langlet Research Center, Hampton, Virginia, 2005.